R. & M. No. 3710

MINISTRY OF DEFENCE (PROCUREMENT EXECUTIVE)

AERONAUTICAL RESEARCH COUNCIL
REPORTS AND MEMORANDA

Theoretical Calculation of Generalised Forces and Load Distribution on Wings Oscillating at General Frequency in a Subsonic Stream

By Doris E. Lehrian and H. C. Garner

Aerodynamics Dept., R.A.E. Teddington
(with Appendices by A. R. Curtis and W. E. A. Acum and by P. S. Hampton)
N. P. L. Teddington

LONDON: HER MAJESTY'S STATIONERY OFFICE
1973
PRICE £2·65 NET

Theoretical Calculation of Generalised Forces and Load Distribution on Wings Oscillating at General Frequency in a Subsonic Stream

By Doris E. Lehrian and H. C. Garner

Reports and Memoranda No. 3710*
July, 1971

Summary

The theoretical method presented here gives improved accuracy and economy of operation, because it is modelled on a very satisfactory method for steady subsonic flow and is programmed in an efficient machine code for the KDF9 computer. There is no restriction on planform, provided that any cranks are rounded to give smooth leading and trailing edges with continuous curvature. The method is programmed in two parts, illustrated by flow diagrams and an example. An appendix describes various operative schemes for obtaining generalised forces and chordwise loadings in phase and in quadrature with arbitrary wing motion in rigid or elastic modes. Restrictions on size of solution are discussed, and the usable range of chordwise and spanwise parameters should serve most needs.

The method is applied to elliptical, rectangular and tapered swept wings of small and large aspect ratio at Mach numbers up to 0·8 and over a wide range of frequency parameter. Accuracy is established by direct comparison with steady flow, by independent desk calculation, by reverse-flow relationships, by asymptotic expansion for small frequency, and by studies of convergence. Results and computing times compare favourably with those of other collocation methods in current use.

LIST OF CONTENTS

* Replaces R.A.E. Technical Report 71 147-A.R.C. 33 405.

LIST OF CONTENTS—*continued*

1. Introduction

Although the demand for a general linear theoretical treatment of oscillating lifting surfaces stems primarily from requirements for flutter calculations, the objective cannot be achieved without a reliable method to cover special cases of low-frequency stability derivatives and the loading on thin wings in steady flow. Moreover, a method that is satisfactory over the whole frequency spectrum is applicable to problems of time-dependent flow involving gust and response functions.

The problem of calculating the aerodynamic load distribution on a wing in harmonic motion in a uniform subsonic stream has long been the subject of mathematical analysis and programming for automatic calculation. The present contribution in this field is based on linear theory and is intended to provide the improved accuracy and economy of operation that can be achieved respectively by modelling the theory on a very satisfactory method for steady flow, and by using an efficient machine code.

The historical sequence leading to the present investigation has been an iterative one, in the course of which subsonic lifting-surface methods have been extended from zero to small frequency, from small to general frequency, and have then been found wanting in greater or lesser degree. The failings have arisen from imperfections in numerical techniques in steady flow, which have to some extent been remedied. The cycle has repeated itself more than once.

As a first generation, we may consider Refs. 1 to 4. Multhopp's[1] theory, extended to low frequency in Ref. 2, was developed for general frequency by Acum[3] and Davies[4]. Both Refs. 3 and 4 are based on the kernel function of the downwash integral due to Watkins *et al.*[5]; in practical operation they differ in that Ref. 3 includes collocation points along the centre line, while Ref. 4 has avoided this situation. It was discovered that all four methods suffer from an integration routine that gives inaccurate downwash over, say, the front quarter chord of the wing when the loading at the leading edge has the usual inverse-square root singularity. None of them could therefore be expected to have sufficient accuracy if the number of chordwise terms were increased above 2 or 3; this becomes more and more desirable as the frequency parameter grows.

Downwash studies in steady flow then led to the low-frequency theory of Garner and Fox[6], and later to a corresponding improved method for general frequency by Long[7]. Just as Ref. 6 superseded Ref. 2 and became available as a program in Algol 60, so Ref. 7 became an improved version of Ref. 4 re-programmed in Fortran IV. The innovation in this second generation was an additional parameter to control the spanwise integration following the chordwise integration of the downwash integral. While these methods are in current use and give desirable improvement in accuracy, which is sufficient for many purposes, some limitations persist. Unfavourable conditions arise when particularly large numbers of chordwise terms are needed; convergence with respect to the spanwise integration parameter is then markedly slower, especially for wings of high aspect ratio typical of many civil aircraft. Although Ref. 6 is restricted to at most four chordwise terms, Ref. 7 is not limited in this way; nevertheless, converged results for very high frequency or high-order chordwise bending would require many more chordwise terms and consequent downwash points so near the leading edge as to demand excessive spanwise integration points.

The sequel in steady flow is reassuring. Zandbergen *et al.*[8] and also Hewitt and Kellaway[9] have developed new and more efficient approaches to the evaluation of the downwash integral. Moreover, a joint investigation involving solutions by the methods of Refs. 6, 8 and 9 for selected planforms at uniform incidence has been published in Ref. 10. The best solutions by each of the three methods show excellent agreement, but there is sufficient evidence to discourage the extension of Ref. 6 to more than four chordwise terms, while Refs. 8 and 9 should remain satisfactory for larger numbers. The present method for general frequency is an offspring of Refs. 3 and 8. The influence functions used by Acum and the spanwise integration routine of Zandbergen *et al.* are combined. After some mathematical manipulation the resulting equations are programmed in KDF9 Usercode to determine generalised forces with arbitrary modes and load distributions at arbitrary sections for any choice of planform, subsonic Mach number and frequency parameter.

The re-formulated equations give numerical results consistent with those of Ref. 8 in the limiting case of steady flow. The new program has been checked by hand calculation for an illustrative example for

moderately high Mach number and frequency parameter. Reverse-flow checks are applied, and comparison is made with several current theories for general frequency. The main applications are to wings of low and moderately high aspect ratio and cover a wide range of frequency parameter, convergence with respect to the number of chordwise terms being studied in both cases. The method is well suited to determine gust and response functions relating to the aerodynamic loading in time-dependent flow.

2. Formulation in Steady Flow

In presenting the principles and basic equations of Ref. 8, it is necessary to change the notation. This will facilitate the use of Ref. 3 and avoid repetition of equations in the following Section 3. We take the origin at a reference point on the centre line of the planform with x-axis horizontal along the stream of uniform velocity U and density ρ, y-axis to starboard and z-axis vertically upwards. The wing is of zero thickness and slightly displaced from the plane $z = 0$. The linearised boundary condition on $z = 0$ expresses the local upwash angle as

$$\frac{w(x, y)}{U} = -\frac{1}{8\pi}\int_{-s}^{s}\int_{x_l(\eta')}^{x_t(\eta')} l(x', y')K(x, y; x', y')\,dx'\,dy', \tag{1}$$

where s is the semi-span of the wing, $x_l(\eta')$ and $x_t(\eta')$ with $\eta' = y'/s$ define its leading and trailing edges, l denotes lift per unit area as a fraction of the dynamic pressure $\frac{1}{2}\rho U^2$ and the kernel function is given by

$$K(x, y; x', y') = -\frac{1}{(y - y')^2}\left[1 + \frac{x - x'}{\{(x - x')^2 + \beta^2(y - y')^2\}^{\frac{1}{2}}}\right], \tag{2}$$

where $\beta^2 = 1 - M^2$ and M is the subsonic Mach number of the stream.

In choosing the standard form of $l(x', y')$ it is supposed that $x_l(\eta')$ and $x_t(\eta')$ are smooth functions to give a 'regular' planform. Then we can write

$$l(x', y') = \frac{8s}{\pi c(\eta')}\sum_{q=1}^{N}\Gamma_q(\eta')\Psi_q(\phi'), \tag{3}$$

where $c(\eta')$ is the wing chord, the spanwise distributions $\Gamma_q(\eta')$ are to be determined,

$$\Psi_q(\phi') = \frac{\cos(q - 1)\phi' + \cos q\phi'}{\sin\phi'} \tag{4}$$

and the angular chordwise parameter ϕ' is given by

$$x' = x_l(\eta') + \tfrac{1}{2}c(\eta')(1 - \cos\phi'). \tag{5}$$

With the substitution of equations (3) to (5) the upwash integral in equation (1) can be written as

$$\frac{w(x, y)}{U} = \frac{1}{2\pi}\sum_{q=1}^{N}\int_{-1}^{1}\frac{\Gamma_q(\eta')F_q(x, \eta; \eta')}{(\eta - \eta')^2}\,d\eta' \tag{6}$$

in terms of 'influence functions' $F_q(x, \eta; \eta')$, which are integrals with respect to ϕ'. It follows from equation (2) that the functions F_q are conveniently expressed in terms of the two non-dimensional parameters

$$\left.\begin{aligned} X &= \frac{x - x_l(\eta')}{c(\eta')} \\ Y &= \frac{\beta s|\eta - \eta'|}{c(\eta')} \end{aligned}\right\}; \tag{7}$$

thus

$$F_q(x,\eta;\eta') = \frac{1}{\pi}\int_0^{\pi}\left[1 + \frac{X - X_0}{\{(X-X_0)^2 + Y^2\}^{\frac{1}{2}}}\right]\Psi_q(\phi')\sin\phi'\,d\phi' \tag{8}$$

where $X_0 = \frac{1}{2}(1 - \cos\phi')$.

The integrand of equation (6) has a strong singularity at $\eta' = \eta$, which has to be accounted for by taking the second-order principal value as derived by Mangler in Appendix I of Ref. 1. Furthermore, the logarithmic singularity inherent in the integrand of equation (6) is removed by taking

$$P_q(x,\eta;\eta') = F_q(x,\eta;\eta') - \left(\frac{\beta s}{c(\eta)}\right)^2 E_q(x,\eta)(\eta - \eta')^2 \ln|\eta - \eta'|, \tag{9}$$

where $E_q(x,\eta)$ is discussed later in Section 2. By means of equation (9), the upwash integral of equation (6) is rewritten as

$$\frac{w(x,y)}{U} = \frac{1}{2\pi}\sum_{q=1}^{N}\left[\int_{-1}^{1}\frac{\Gamma_q(\eta')P_q(x,\eta;\eta')}{(\eta-\eta')^2}\,d\eta' + \left(\frac{\beta s}{c(\eta)}\right)^2\left\{E_q(x,\eta)\int_{-1}^{1}\Gamma_q(\eta')\ln|\eta-\eta'|\,d\eta'\right\}\right]. \tag{10}$$

The above equations provide the basis of Multhopp's[1] method and its subsequent developments for steady or oscillatory flow in Refs. 3, 6 and 8 for example. The solution of equation (10) for the spanwise distributions $\Gamma_q(\eta')$ due to a given wing displacement $z(x, y)$ is achieved by collocation at specified upwash points $x = x_{pv}$ and $y = y_v$ on the wing planform.

A basic difference between Ref. 8 and earlier methods for steady flow is that in the product $\Gamma_q(\eta')P_q(x,\eta;\eta')$ of equation (10) the two functions are treated separately. The accuracy of the numerical procedure for the first integral in equation (10) is improved by the construction of a 'regularised' influence function $R_q(x,\eta;\eta')$, which may be represented by a higher-order polynomial than the loading $\Gamma_q(\eta')$. The spanwise distribution is represented by the double Fourier series

$$\Gamma_q(\eta') = \frac{2}{m+1}\sum_{r=1}^{m}\left[\Gamma_{qr}\sum_{\mu=1}^{m}\sin\mu\theta'\sin\mu\theta_r\right] \tag{11}$$

where $\eta' = -\cos\theta'$; the values $\Gamma_{qr} = \Gamma_q(\eta_r)$ correspond to the stations

$$\eta_r = -\cos\theta_r = -\cos\left(\frac{r\pi}{m+1}\right), \qquad r = 1(1)m, \tag{12}$$

and the integer m can be either even or odd. The regularised influence function $R_q(x,\eta;\eta')$ is constructed according to equations (A(2) and A(3) of Ref. 8 and becomes

$$R_q(x,\eta;\eta') = \sin\theta'\left\{\frac{P_q(x,\eta;\eta') - P_q(x,\eta;\eta) - (\eta'-\eta)P'_q(x,\eta;\eta)}{(\eta'-\eta)^2}\right\}, \tag{13}$$

where

$$\left.\begin{aligned} P'_q(x,\eta;\eta) &= \left[\frac{\partial P_q(x,\eta;\eta')}{\partial\eta'}\right]_{\eta'=\eta} \\ \text{and by equation (9)} \qquad P_q(x,\eta;\eta) &= F_q(x,\eta;\eta) \end{aligned}\right\}. \tag{14}$$

The numerator in equation (13) is of order $(\eta' - \eta)^2$ in the neighbourhood of $\eta' = \eta$, so that the function $R_q(x,\eta;\eta')$ is bounded and continuous and can be represented adequately as in equation A(4) of Ref. 8 by

$$R_q(x,\eta;\eta') = \frac{2}{\Lambda+1}\sum_{\lambda=1}^{\Lambda}\left[R_q(x,\eta;\eta_\lambda)\sum_{\omega=1}^{\Lambda}\sin\omega\theta'\sin\omega\theta_\lambda\right], \tag{15}$$

where

$$\left.\begin{aligned} \eta_\lambda &= -\cos\theta_\lambda = -\cos\left(\frac{\lambda\pi}{\Lambda+1}\right), \qquad \lambda = 1(1)\Lambda \\ \Lambda &= \{a(m+1)-1\} \\ a &= \text{positive integer} \end{aligned}\right\}. \tag{16}$$

By taking the parameter a sufficiently large, we can achieve any desired accuracy in the representation of $R_q(x, \eta; \eta')$ to be used in equation (13). When the integrals in equation (10) are transformed to the variable θ' with the substitution of $\Gamma_q(\eta')$ from equation (11) and $P_q(x, \eta; \eta')$ from equations (13) and (15), a tractable form is obtained for $w(x, y)$.

In the present method, the number and position of the upwash points $x = x_{pv}$, $y = y_v$ are restricted to the Nm values given by

$$\left.\begin{aligned} x_{pv} &= x_l(\eta_v) + \tfrac{1}{2}c(\eta_v)\{1 - \cos\phi_p\} = x_{lv} + \tfrac{1}{2}c_v(1 - \cos\phi_p) \\ \phi_p &= 2\pi p/(2N+1), \qquad p = 1(1)N \end{aligned}\right\} \tag{17}$$

and

$$\eta_v = y_v/s = -\cos\theta_v = -\cos\left(\frac{v\pi}{m+1}\right), \qquad v = 1(1)m. \tag{18}$$

The integrals remaining in the upwash $w(x_{pv}, y_v)$ are effected analytically with due regard to the principal value and are denoted here as coefficients $\kappa_{r\lambda}, \rho_{vr}, \sigma_{vr}, \tau_{vr}$.* The algebraic formulae for the coefficients with θ_r, θ_λ and θ_v defined according to equations (12), (16) and (18) are

$$\left.\begin{aligned} \kappa_{r\lambda} &= \frac{(-1)^r \sin\theta_r \sin(\lambda\pi/a)}{2(m+1)(\Lambda+1)(\cos\theta_\lambda - \cos\theta_r)} && \theta_\lambda \neq \theta_r \\ &= -\frac{1}{2(\Lambda+1)} && \theta_\lambda = \theta_r, \text{ i.e., } \lambda = ar \end{aligned}\right\}, \tag{19}$$

$$\left.\begin{aligned} \rho_{vr} &= -\frac{\sin\theta_r\{1 - (-1)^{r+v}\}}{2(m+1)(\cos\theta_v - \cos\theta_r)^2} && \theta_r \neq \theta_v \\ &= \frac{(m+1)}{4\sin\theta_v} && \theta_r = \theta_v \end{aligned}\right\}, \tag{20}$$

$$\left.\begin{aligned} \sigma_{vr} &= -\frac{\sin\theta_r\{1 - (-1)^{r+v}\}}{2(m+1)(\cos\theta_v - \cos\theta_r)} && \theta_r \neq \theta_v \\ &= 0 && \theta_r = \theta_v \end{aligned}\right\}, \tag{21}$$

and

$$\tau_{vr} = -\frac{1}{m+1}\left[\sin\theta_r(\tfrac{1}{4}\cos 2\theta_v - \tfrac{1}{2}\ln 2) - \sum_{\mu=2}^{m}\frac{\{\mu\sin\mu\theta_v \sin\theta_v + \cos\mu\theta_v\cos\theta_v\}\sin\mu\theta_r}{(\mu^2-1)}\right]. \tag{22}$$

---

* These correspond to the four integrals defined in equations A(6)(a to d) of Ref. 8 after multiplication by the respective factors

$$-\frac{1}{2a(m+1)}, \quad -\frac{\sin\theta_r}{2\sin\theta_v}, \quad -\tfrac{1}{2}, \quad -\tfrac{1}{2} \text{ and the substitution } \theta_r \text{ for } \theta_n.$$

The values of the coefficients ρ_{vr}, σ_{vr} and τ_{vr} are governed solely by the value m chosen for the collocation solution, whilst the values of $\kappa_{r\lambda}$ depend also on the value assigned to Λ through the integer a of equation (16). Formulation of $w(x_{pv}, y_v)$ at the points given by equations (17) and (18) therefore provides a set of Nm linear equations in the unknown coefficients Γ_{qr}; thus

$$-\frac{w(x_{pv}, y_v)}{U} = \sum_{q=1}^{N} \sum_{r=1}^{m} \Gamma_{qr} \Omega_q(p, v, r) \tag{23}$$

with

$$\Omega_q(p, v, r) = \left[\sum_{\lambda=1}^{\Lambda} \{R_q(p, v, \lambda)\kappa_{r\lambda}\} + P_q(p, v)\rho_{vr} + P'_q(p, v)\sigma_{vr} + \left(\frac{\beta s}{c_v}\right)^2 E_q(p, v)\tau_{vr} \right], \tag{24}$$

where the abbreviated notation (p, v, λ), (p, v) indicates that the function corresponds to the values $(x_{pv}, \eta_v; \eta_\lambda)$, $(x_{pv}, \eta_v; \eta_v)$ respectively.

The major part of the computation for $\Omega_q(p, v, r)$ is in the evaluation of the regularised influence functions from equation (13) rewritten as

$$R_q(p, v, \lambda) = \sin\theta_\lambda \left\{ \frac{P_q(p, v, \lambda) - P_q(p, v) - (\eta_\lambda - \eta_v)P'_q(p, v)}{(\eta_\lambda - \eta_v)^2} \right\}, \tag{25}$$

$$\text{for } q = 1(1)N,\ p = 1(1)N,\ v = 1(1)m,\ \lambda = 1(1)\Lambda,$$

where by equation (9)

$$\left.\begin{aligned} P_q(p, v, \lambda) &= F_q(x_{pv}, \eta_v; \eta_\lambda) - \left(\frac{\beta s}{c_v}\right)^2 E_q(p, v)(\eta_v - \eta_\lambda)^2 \ln|\eta_v - \eta_\lambda| \\ P_q(p, v) &= F_q(x_{pv}, \eta_v; \eta_v) \\ P'_q(p, v) &= P'_q(x_{pv}, \eta_v; \eta_v), \text{ defined by equation (14)} \end{aligned}\right\}. \tag{26}$$

For steady flow the required values of the influence functions $F_q(x_{pv}, \eta_v; \eta_\lambda)$ are determined by equations (4) and (8) where in place of equation (7)

$$\left.\begin{aligned} X(p, v, \lambda) &= \frac{x_{pv} - x_l(\eta_\lambda)}{c(\eta_\lambda)} = \frac{x_{pv} - x_{l\lambda}}{c_\lambda} \\ Y(v, \lambda) &= \frac{\beta s|\eta_v - \eta_\lambda|}{c_\lambda} \end{aligned}\right\}. \tag{27}$$

The particular value $R_q(p, v; \lambda = av)$ requires a special formula, since equation (25) is indeterminate when $\eta_\lambda = \eta_v$.

The series development of F_q from equation (8) with fixed X and small Y is of the form

$$F_q = F_q(X, Y = 0) + \{Y^2 \ln Y\}\{E_q(X) + O(Y^2)\} + Y^2\{D_q(X) + O(Y^2)\}, \tag{28}$$

where $E_q(X)$ is equivalent to the quantity $E_q(x, \eta)$ introduced in equation (9). It follows from equations (4) and (8) that

$$F_q(X, Y = 0) = \frac{2}{\pi}\int_0^\phi \Psi_q(\phi') \sin\phi' \, d\phi' \tag{29}$$

where $X = \frac{1}{2}(1 - \cos\phi)$. We write

$$\left.\begin{aligned} F_q(X, Y = 0) = 2L_q(X) &= \frac{2}{\pi}[\phi + \sin\phi], && q = 1 \\ &= \frac{2}{\pi}\left[\frac{\sin(q-1)\phi}{q-1} + \frac{\sin q\phi}{q}\right], && q \geqslant 2 \end{aligned}\right\}. \tag{30}$$

Differentiation with respect to X gives

$$L_q'(X) = \frac{2}{\pi}\left[\frac{\cos(q-1)\phi + \cos q\phi}{\sin\phi}\right]. \tag{31}$$

From the analysis in Appendix III of Ref. 1, it is easily shown that

$$E_q(X) = -L_q''(X) = \frac{4}{\pi}\left[\frac{q\cos(q-1)\phi - (q-1)\cos q\phi}{\sin\phi(1-\cos\phi)}\right]. \tag{32}$$

An algebraic formula for $D_q(X)$ can be deduced from equation A(18) of Ref. 8 to be

$$\begin{aligned} D_q(X) = &-\frac{q\sin(q-1)\phi - (q-1)\sin q\phi}{X\sin\phi} + \frac{2}{\pi X}[qI_{q-1} - (q-1)I_q] \\ &+ X^{-1}L_q'(X) + L_q''(X)[\tfrac{1}{2} + \ln\{8X(1-X)\}], \end{aligned} \tag{33}$$

where $I_0 = 0$, $I_1 = (\pi - \phi)$ and there is the recurrence relation

$$I_q - (2\cos\phi)I_{q-1} + I_{q-2} = -\frac{2}{q-1}\sin(q-1)\phi, \qquad q \geqslant 2.$$

In practice, $D_q(X)$ has been calculated from the integral expression in equation (I.23) of Appendix I for general frequency; in the special case of steady flow ($\mu \to 0$) this can be manipulated to give equation (33).

It can be deduced immediately from the limiting form of equation (13) as $\eta' \to \eta$ that

$$R_q(p, v, \lambda = av) = \tfrac{1}{2}P_q''(p, v)\sin\theta_v, \tag{34}$$

where

$$P_q''(p, v) = \left[\frac{\partial^2 P_q(x_{pv}, \eta_v; \eta')}{\partial\eta'^2}\right]_{\eta' = \eta_v}.$$

Substitution of equation (28) into equation (9) gives an expansion for $P_q(x, \eta; \eta')$; after differentiation with respect to η'

$$\begin{aligned} P_q'(x, \eta; \eta') = J(\eta')\frac{dF_q(X, Y = 0)}{dX} &+ \frac{\partial Y}{\partial\eta'}[\{Y + 2Y\ln Y\}E_q(X) + 2YD_q(X)] \\ &+ \left[\frac{\beta s}{c(\eta)}\right]^2\{(\eta - \eta') + 2(\eta - \eta')\ln|\eta - \eta'|\}E_q(X) + O(Y^3\ln Y), \end{aligned} \tag{35}$$

where by equation (7) for X

$$J(\eta') = \frac{\partial X}{\partial\eta'} = -\frac{x_1'(\eta') + Xc'(\eta')}{c(\eta')} \tag{36}$$

in terms of the differential coefficients $x_l'(\eta')$ and $c'(\eta')$. Differentiation of equation (35) gives

$$P_q''(x, \eta; \eta') = J'(\eta')\frac{dF_q(X, Y=0)}{dX} + \{J(\eta')\}^2\frac{d^2F_q(X, Y=0)}{dX^2}$$
$$+ \left(\frac{\partial Y}{\partial \eta'}\right)^2 [\{3 + 2\ln Y\}E_q(X) + 2D_q(X)]$$
$$- \left[\frac{\beta s}{c(\eta)}\right]^2 \{3 + 2\ln|\eta - \eta'|\}E_q(X) + O(Y^2 \ln Y) \tag{37}$$

where, since

$$\left(\frac{\partial Y}{\partial \eta'}\right)^2 = \left[\frac{\beta s}{c(\eta')}\right]^2 + O(Y),$$

it can be seen that the logarithmic singularities will cancel when $\eta' \to \eta$. With substitutions $x = x_{pv}$ and $\eta' \to \eta = \eta_v$, equations (7) become

$$\left.\begin{aligned} X &= X_p = \tfrac{1}{2}(1 - \cos\phi_p) \\ Y &= 0 \end{aligned}\right\}, \tag{38}$$

and equations (9), (31) and (35) reduce to

$$\left.\begin{aligned} P_q(p, v) &= 2L_q(X_p) \\ P_q'(p, v) &= 2J_{pv}L_q'(X_p) \end{aligned}\right\}. \tag{39}$$

Similarly equations (34), (36) and (37) reduce to give the required limiting form of equation (25)

$$R_q(p, v, \lambda = av) = \sin\theta_v\left[J_{pv}'L_q'(X_p) + J_{pv}^2L_q''(X_p) + \left(\frac{\beta s}{c_v}\right)^2\left\{D_q(X_p) + E_q(X_p)\ln\left(\frac{\beta s}{c_v}\right)\right\}\right], \tag{40}$$

where

$$\left.\begin{aligned} J_{pv} &= -\frac{x_{lv}' + X_p c_v'}{c_v} \\ J_{pv}' &= -\frac{x_{lv}'' + X_p c_v'' + 2J_{pv}c_v'}{c_v} \end{aligned}\right\}. \tag{41}$$

The regularised influence functions R_q are thus defined by equation (25) or (40), where F_q, P_q and its limiting value and derivative are given in equations (8) and (26); the formulation also includes the supplementary functions $L_q(X_p)$ and its derivatives, $E_q(p, v) \equiv E_q(X_p)$, $D_q(X_p)$, J_{pv} and J_{pv}' from equations (30) to (33) and (38) to (41).

We can now return to equations (19) to (24) and relate the upwash angle to an arbitrary mode of deformation by means of

$$\frac{w}{U} = \left(\frac{w}{U}\right)_j = \frac{\partial z_j}{\partial x}, \tag{42}$$

where $z_j(x, y)$ denotes an upward displacement of the wing. Equation (23) may then be rewritten as

$$\sum_{q=1}^{N}\sum_{r=1}^{m}\Omega_q(p, v, r)(\Gamma_{qr})_j = -\frac{\partial z_j}{\partial x}(x_{pv}, y_v), \tag{43}$$

where the coefficients $\Omega_q(p, v, r)$ from equation (24) form a square matrix of order mN. It remains to solve the linear simultaneous equations for $(\Gamma_{qr})_j$ and to substitute in equation (3) for the wing loading

$$(l_r)_j = \frac{8s}{\pi c_r} \sum_{q=1}^{N} (\Gamma_{qr})_j \Psi_q(\phi) \tag{44}$$

at the sections in equation (12) where

$$x = x_{lr} + \tfrac{1}{2}c_r(1 - \cos\phi), \qquad r = 1(1)m. \tag{45}$$

In general, there are force modes $z = z_i(x, y)$ and force coefficients

$$Q_{ij} = -\frac{1}{2dD} \int_S \int z_i l_j \, dx \, dy, \tag{46}$$

where d and D are the arbitrary reference length and area respectively and

$$l_j = \frac{8s}{\pi c(\eta)} \sum_{q=1}^{N} [\Gamma_q(\eta)]_j \frac{\cos(q-1)\phi + \cos q\phi}{\sin\phi} \tag{47}$$

with spanwise distributions $[\Gamma_q(\eta)]_j$ in accord with equation (11). With $D = S$ and $z_i = z_1 = -d$, for example, equations (46) and (47) reduce to

$$Q_{1j} = \tfrac{1}{2}C_L = \frac{\pi A}{2(m+1)} \sum_{r=1}^{m} (\Gamma_{1r})_j \sin\frac{r\pi}{m+1}, \tag{48}$$

where C_L is the lift coefficient and $A = (2s)^2/S$ is the aspect ratio of the planform. Similarly, with $z_i = z_2 = -x$

$$Q_{2j} = -\tfrac{1}{2}C_m = \frac{\pi A}{2(m+1)d} \sum_{r=1}^{m} \{(\Gamma_{1r})_j (x_{lr} + \tfrac{1}{4}c_r) - (\Gamma_{2r})_j (\tfrac{1}{4}c_r)\} \sin\frac{r\pi}{m+1}, \tag{49}$$

where C_m is the nose-up pitching moment coefficient about the axis $x = 0$ with arbitrary reference length d.

The requirement, that the planform is regular, is closely allied to equation (41) for J'_{pv} with its explicit dependence on the second derivatives x''_{lv} and c''_v. It is necessary that the planform should have continuous curvature at the collocation sections; moreover, it is desirable to remove irregularities due to cranks wherever they occur (Section 4.1). Given a smooth planform, the subsonic Mach number and modes z_i and z_j, there are still the basic parameters N, m and a to specify the collocation points and the terms in the loading and to ensure sufficient accuracy in equation (15); some guidance is found in Section 4.3. In Section 5.1 there is numerical confirmation that a solution of the preceding equations is consistent with results obtained for steady flow in the original Ref. 8. Many of these equations continue to apply in the formulation for general frequency that follows in Section 3, although the details are much more complicated.

3. Extension to General Frequency

For lifting surfaces oscillating in simple harmonic modes at an angular frequency ω, linearized theory applies subject to the limitations indicated in Section 2 and provided that the oscillations are of small amplitude about zero mean incidence or a steady state within the scope of Ref. 8. As can be seen from equations (24) to (27) of Ref. 3, the integral equation relating the complex upwash $w(x, y)\,e^{i\omega t}$ and the complex load distribution $l(x', y')\,e^{i\omega t}$ over the wing planform at time t has the same form as equation (1) but with an oscillatory kernel function $K(x, y; x', y')$ dependent also upon ω and M. As in the theory of

Ref. 3, it is convenient to take

$$w(x, y) = \exp\{-i\bar{\nu}x/\bar{c}\}\bar{w}(x, y) \tag{50}$$

and

with

$$\left.\begin{aligned} l(x', y') &= \exp\{-i\bar{\nu}x/\bar{c}\}\bar{l}(x, y) \\ \bar{l}(x', y') &= \frac{8s}{\pi c(\eta')} \sum_{q=1}^{N} [\Gamma_q(\eta')\Psi_q(\phi')] \end{aligned}\right\} \tag{51}$$

where $\bar{\nu} = \omega\bar{c}/U$ in terms of the geometric mean chord $\bar{c}$ and the real chordwise distributions $\Psi_q(\phi')$ are given by equations (4) and (5). Again it is assumed that the spanwise distribution $\Gamma_q(\eta')$ is smooth over the wing span and can be represented by the interpolation polynomial of equation (11) with unknown coefficients Γ_{qr}, these now being the complex values $\Gamma_q(\eta_r)$. Equations (51) with $\bar{\nu} = 0$ give $l(x', y')$ consistent with the load distribution for steady flow in equation (3).

The integral equation of the upwash $w(x, y)$ for general $\bar{\nu}$ reduces by means of equations (50) and (51) to an equation for the modified upwash

$$\frac{\bar{w}(x, y)}{U} = \frac{1}{2\pi} \sum_{q=1}^{N} \int_{-1}^{1} \frac{\Gamma_q(\eta')F_q(x, \eta; \eta')}{(\eta - \eta')^2}\, d\eta' \tag{52}$$

with

$$\Gamma_q(\eta') = \frac{2}{(m+1)} \sum_{r=1}^{m} \left[\Gamma_{qr} \sum_{\mu=1}^{m} (\sin\mu\theta' \sin\mu\theta_r)\right] \tag{53}$$

where $\eta' = -\cos\theta'$ and $\eta_r = -\cos\{r\pi/(m+1)\}$, $r = 1(1)m$. The oscillatory influence functions F_q are defined as

$$F_q(x, \eta; \eta') = -\frac{1}{\pi}\int_0^{\pi} \left[(y - y')^2 \exp\left\{\frac{i\bar{\nu}(x - x')}{\bar{c}}\right\} K(x, y; x', y')\right] \Psi_q(\phi') \sin\phi'\, d\phi' \tag{54}$$

with the modified kernel function in the square brackets corresponding to the function defined by equations (68) to (72) of Ref. 3 and used in Appendix I. From the point of view of programming, it is convenient to express F_q as a function of the five non-dimensional parameters

$$M, \bar{\nu}, \frac{c(\eta')}{\bar{c}}, X \text{ and } Y,$$

with the two non-dimensional coordinates defined by equation (7). The form of the function F_q in the neighbourhood of $Y = 0$ is shown by equation (126) of Ref. 3; its extension in Appendix I of the present Report is similar to the series developed in equation (28) for small Y, but with the functions $F_q(X, Y = 0)$, $E_q(X)$ and $D_q(X)$ appropriate to the oscillatory problem. By equation (90) of Ref. 3, $F_q(X, Y = 0)$ is independent of $\bar{\nu}$ and in fact identical to equation (30). By equation (127) of Ref. 3,

$$E_q(X) = [-L_q''(X) + 2i\mu L_q'(X) + \beta^2\mu^2 L_q(X)] \tag{55}$$

in terms of the functions defined by equations (30) to (32) and with

$$\mu = \frac{\bar{\nu}c(\eta')}{\beta^2\bar{c}}. \tag{56}$$

The function $D_q(X)$ is the complicated sum of integrals in equation (I.23) which is also dependent upon μ and has to be computed numerically.

Now we consider the integration for the modified upwash in equation (52). The resemblance between the form of the integral for $\bar{w}(x, y)$ and that for the upwash $w(x, y)$ in steady flow from equation (6) indicates that the procedures of Section 2 may be applied directly to the evaluation of the modified upwash for general frequency. It can be shown that a collocation solution for the oscillatory coefficients Γ_{qr} leads to a set of Nm linear equations for $\bar{w}(x_{pv}, y_v)$, similar to equation (23) and with complex elements $\Omega_q(p, v, r)$ now defined by equations (24) to (26) in terms of $F_q(x_{pv}, \eta_v; \eta_\lambda)$ from equation (54) and $E_q(p, v)$ from equation (55) with the substitutions

$$\left.\begin{aligned} X = X_p &= \frac{1}{2}\left(1 - \cos\frac{2\pi p}{2N+1}\right) \\ \mu = \mu_v &= \frac{\bar{\nu} c_v}{\beta^2 \bar{c}} \end{aligned}\right\} \tag{57}$$

consistent with the collocation points in equations (17) and (18). The limiting form of the regularized influence function

$$R_q(p, v, \lambda = av) = \sin\theta_v\left[J'_{pv}L'_q(X_p) + J^2_{pv}L''_q(X_p) + \left(\frac{\beta s}{c_v}\right)^2\left\{D_q(p, v) + E_q(p, v)\ln\frac{\beta s}{c_v}\right\}\right] \tag{58}$$

is unchanged from equation (40), except that the quantities $D_q(p, v)$ and $E_q(p, v)$ denote their dependence on both chordwise and spanwise location of the upwash point through X_p and the local frequency parameter μ_v from equations (57).

The boundary condition and wing loading for arbitrary modes in equations (42) to (49) no longer apply when the flow is oscillatory. The modified upwash from equation (50) is obtained from the upward displacement mode $z_j(x, y)$ as

$$\frac{\bar{w}_j(x, y)}{U} = \exp\left\{\frac{i\bar{\nu}x}{\bar{c}}\right\}\frac{w_j(x, y)}{U} = \exp\left\{\frac{i\bar{\nu}x}{\bar{c}}\right\}\left[\frac{\partial z_j}{\partial x} + \frac{i\bar{\nu}z_j}{\bar{c}}\right]. \tag{59}$$

In place of equation (23), the complex set of equations to be solved for $(\Gamma_{qr})_j$ is

$$\sum_{q=1}^{N}\sum_{r=1}^{m}\Omega_q(p, v, r)(\Gamma_{qr})_j = (h_{pv})_j = -\frac{\bar{w}_j(x_{pv}, y_v)}{U}, \tag{60}$$

where $\Omega_q(p, v, r)$ is still formulated from equation (24), $p = 1(1)N$ and $v = 1(1)m$. Hence the complex loading from equations (51) is obtainable at each collocation section as

$$(l_r)_j = \frac{8s}{\pi c_r}\exp\left\{-\frac{i\bar{\nu}x}{\bar{c}}\right\}\sum_{q=1}^{N}(\Gamma_{qr})_j\Psi_q(\phi), \tag{61}$$

where x and ϕ are related by equation (45). The complete distribution l_j follows by writing $c(\eta)$ for c_r and replacing $(\Gamma_{qr})_j$ by $[\Gamma_q(\eta)]_j$ in accord with equation (11). The generalised force coefficients are then defined as before by the surface integral (46), which after chordwise integration becomes

$$Q_{ij} = \frac{2s^2}{\pi D}\sum_{q=1}^{N}\int_{-1}^{1}[\Gamma_q(\eta)]_j K_{iq}\,d\eta \tag{62}$$

with

$$K_{iq} = -\exp\left\{-\frac{i\bar{\nu}(x_l + \frac{1}{2}c)}{\bar{c}}\right\}\int_0^\pi \frac{z_i}{d}\exp\left\{\frac{i\bar{\nu}c\cos\phi}{2\bar{c}}\right\}\Psi_q(\phi)\sin\phi\, d\phi. \tag{63}$$

For the simple modes z_i considered in equations (48) and (49), the integrals K_{iq} are expressible in terms of Bessel functions as indicated in equations (149) and (150) of Ref. 3. In practice, however, equation (63) is evaluated by numerical integration. The final spanwise integration in equation (62) is accomplished by application of the interpolation polynomial (11) to the product $\Gamma_q K_{iq}$, which presupposes that K_{iq} can be represented by a polynomial in η of order less than m. It is then sufficient to calculate

$$Q_{ij} = \frac{2s^2}{D(m+1)}\sum_{q=1}^{N}\sum_{r=1}^{m}(\Gamma_{qr})_j(K_{qr})_i\sin\theta_r, \tag{64}$$

where $(K_{qr})_i$ denotes the value of K_{iq} at the section $\eta = -\cos\theta_r$ defined in equation (12). Table II.4a of Appendix II shows how provision is made to output $(K_{qr})_i$, if required.

The summations with respect to r in equations (60) and (64) can be roughly halved in length as soon as it is known whether the spanwise loading is symmetrical or antisymmetrical and whether m, the number of collocation sections from tip to tip, is even or odd. The major part of the calculation lies in evaluating the elements $\Omega_q(p, \nu, r)$ of the aerodynamic influence matrix, and the success of the computer program depends in large measure on the efficient handling of this process in KDF9 Usercode. There are particular quantities λ_{int} and κ that are set to optimise the calculation of the complicated function $D_q(p, \nu)$ required in equation (58) and derived in Appendix I. There are, moreover, the variable parameters δ and ε that limit the smallness of interval in spanwise integration and control the tolerance in accuracy (Appendix II). It is remarkable that the computation time for general frequency is less than twice that for steady flow, unless the frequency parameter is very large (say, $\bar{\nu} > 9\beta^2$).

4. Numerical and Program Data for KDF9

The preceding formulation has presupposed than the planform is smooth apart from the possibility of a pointed or steamwise tip. Elsewhere on the planform, discontinuities in slope require the artificial rounding discussed in Section 4.1. The modes of oscillation are chosen and defined according to Section 4.2. Section 4.3 gives recommended values of the other parameters needed to specify the basic calculation. Solution by collocation can then proceed.

As described in Appendix II and illustrated in Appendix III, the method has been programmed in KDF9 Usercode and the calculation can be run on a KDF9 computer in one or two stages. A brief account of Programs I and II and their various uses is given in Section 4.4.

4.1. Planform Data

The derivation of the matrix of ordinary linear simultaneous equations (23) assumes that the leading edge $x_l(\eta)$ and chord $c(\eta)$ are twice differentiable. In practice, planforms with sweepback or taper have discontinuities in slope at the centre section, and likewise at non-central sections if there are cranks or non-streamwise tips. Under such conditions some artificial rounding of the planform becomes necessary.

We consider first a straight-tapered swept wing with streamwise tips. In an arbitrary central region $|\eta| < \eta_{iR}$ the true leading edge and chord are replaced by

$$\left.\begin{aligned} x_l(\eta) &= x_{lR} + f(\lambda)[x_l(\eta_{iR}) - x_{lR}] \\ c(\eta) &= c_R + f(\lambda)[c(\eta_{iR}) - c_R] \end{aligned}\right\} \tag{65}$$

where $0 \leqslant \lambda = |\eta|/\eta_{iR} \leqslant 1$. Of the three shapes of rounding compared in Ref. 10, we choose from Refs. 8

and 9 respectively

$$\left.\begin{aligned} f(\lambda) &= f_1(\lambda) = \tfrac{1}{3} + \lambda^2 - \tfrac{1}{3}\lambda^3 \\ f(\lambda) &= f_2(\lambda) = \tfrac{5}{16} + \tfrac{15}{16}\lambda^2 - \tfrac{5}{16}\lambda^4 + \tfrac{1}{16}\lambda^6 \end{aligned}\right\}. \tag{66}$$

The polynomial $f_1(\lambda)$ is that of the lowest order to achieve continuity in $x_l''(\eta)$ and $c''(\eta)$. The even polynomial $f_2(\lambda)$ gives continuity in the third derivative at $|\eta| = \eta_{iR}$ and in all derivatives at $\eta = 0$. The equation (65) for $c(\eta)$ is conveniently written in the form of an increment

$$c(\eta) = [c(\eta)]_{\text{true}} + g(\lambda)[c(\eta_{iR}) - c_R], \tag{67}$$

where $g(\lambda) = 0$ if $\lambda \geqslant 1$ and from the respective equations (66) when $\lambda \leqslant 1$ either

$$g(\lambda) = g_1(\lambda) = f_1(\lambda) - \lambda = \tfrac{1}{3}(1 - \lambda)^3 \tag{68}$$

or

$$g(\lambda) = g_2(\lambda) = f_2(\lambda) - \lambda = \tfrac{1}{16}(1 - \lambda)^4(5 + 4\lambda + \lambda^2). \tag{69}$$

The rounded leading edge is given by a corresponding increment

$$x_l(\eta) = [x_l(\eta)]_{\text{true}} + g(\lambda)[x_l(\eta_{iR}) - x_{lR}]. \tag{70}$$

Provision has been made to treat four classes of wing denoted by indicators

wing = 1 straight-tapered swept wing with streamwise tips,
wing = 2 straight-edged planform with extra non-central crank at $|\eta| = \eta_K$,
wing = 3 straight-edged planform with cranks at $|\eta| = 0$, η_A and η_B,
wing = 4 planform with leading edge and chord and their first two derivatives specified numerically.

A rectangular wing is treated as a special case of wing = 1, as in equations (67) to (70); although neither has any influence, it is necessary to specify the extent of rounding η_{iR} and shape of rounding, round = 1 or round = 2 from the appropriate equation (68) or (69). In the case wing = 2, equation (67) is replaced by

$$c(\eta) = [c(\eta)]_{\text{true}} + (c_K - c_R)\eta_{iR}g(\lambda_R)/\eta_K, \tag{71}$$

where c_K and c_R are the true crank chord and root chord respectively and $\lambda_R = |\eta|/\eta_{iR}$. To equation (71) is added an increment due to rounding the non-central crank over the region of arbitrary extent $|\eta - \eta_K| \leqslant \eta_{iK}$, so that for $\eta \geqslant 0$

$$c(-\eta) = c(\eta) = [c(\eta)]_{\text{true}} + \frac{c_K - c_R}{\eta_K}\eta_{iR}g(\lambda_R) + \frac{1}{2}\left[\frac{c_T - c_K}{1 - \eta_K} - \frac{c_K - c_R}{\eta_K}\right]\eta_{iK}\{g(\lambda_K) + g(\lambda_{-K})\}, \tag{72}$$

where $\lambda_K = |\eta - \eta_K|/\eta_{iK}$ and the last term with $\lambda_{-K} = |\eta + \eta_K|/\eta_{iK}$ caters for the possibility that the region $|\eta - \eta_K| \leqslant \eta_{iK}$ may extend beyond the root. Similarly in the case wing = 3, the rounded wing chord is given by

$$\begin{aligned} c(-\eta) = c(\eta) = [c(\eta)]_{\text{true}} &+ \frac{c_A - c_R}{\eta_A}\eta_{iR}g(\lambda_R) + \frac{1}{2}\left[\frac{c_B - c_A}{\eta_B - \eta_A} - \frac{c_A - c_R}{\eta_A}\right]\eta_{iA}\{g(\lambda_A) + g(\lambda_{-A})\} \\ &+ \frac{1}{2}\left[\frac{c_T - c_B}{1 - \eta_B} - \frac{c_B - c_A}{\eta_B - \eta_A}\right]\eta_{iB}g(\lambda_B), \end{aligned} \tag{73}$$

where c_R, c_A, c_B are the true chords at $\eta = 0$, η_A, η_B, $\lambda_A = |\eta - \eta_A|/\eta_{iA}$, $\lambda_{-A} = |\eta + \eta_A|/\eta_{iA}$, $\lambda_B = |\eta - \eta_B|/\eta_{iB}$, η_{iA} and η_{iB} ($\leqslant \eta_B$) are arbitrary, $g(\lambda) = 0$ if $\lambda \geqslant 1$ and equations (68) and (69) offer a choice of function $g(\lambda)$. Again there is a corresponding equation for $x_l(-\eta) = x_l(\eta)$. The quantities η_{iR}, η_{iK}, η_{iA} and η_{iB} should normally be of the same order as the spacing between consecutive collocation sections. On the other hand, the two roundings at η_A and η_B might be superposed to simulate a curved tip.

When wing = 1, 2 or 3, it is sufficient to define the planform by numerical values of

$$\text{wing, round, } s,\ x_{lR},\ c_R,\ \eta_{iR},\ x_{lT},\ c_T$$

and intermediate data for each non-central crank, e.g.,

$$\eta_K,\ x_{lK},\ c_K,\ \eta_{iK}.$$

However, wing = 4 caters for planforms with curved edges or with shapes of rounding other than round = 1 or 2. Then every element of planform data to be used in the calculation is input numerically as set out in Table II.2 of Appendix II. The indicator round = 0 implies that the rounding, if any, is different from that of equation (68) or (69).

The origin of coordinates is chosen on the centre line, such that the y-axis becomes the pitching axis. The reference length d is taken as unity and determines the linear scale. The arbitrary reference area D must be specified. The geometric mean chord $\bar{c}$ and associated frequency parameter $\omega\bar{c}/U$ are required, but the aerodynamic mean chord $\bar{\bar{c}}$ and frequency parameter $\omega\bar{\bar{c}}/U$ may replace these without affecting the calculation. The aspect ratio A is not input, but it would normally appear in the descriptive title.

4.2. Mode Data

The mode data fulfil the dual rôle of defining the complex upwash

$$\frac{\bar{w}}{U} = \exp\left\{\frac{i\bar{\nu}x}{\bar{c}}\right\}\left(\frac{\partial z}{\partial x} + \frac{i\bar{\nu}z}{\bar{c}}\right) \tag{74}$$

and the generalised force coefficient

$$Q_i = -\frac{1}{2Dd}\int_{-s}^{s}\int_{x_t(\eta)}^{x_t(\eta)} z_i l(x, y)\, dx\, dy, \tag{75}$$

where $z_i/d = -Z_i$ is the force mode. The oscillatory motion is expressed in terms of a linear combination of modes as an upward deflection

$$z(x, y) = -d\sum_{j=1}^{J} b_j Z_j(x/d, y/s). \tag{76}$$

There are corresponding expressions for the non-dimensional loading

$$l(x, y) = \sum_{j=1}^{J} b_j l_j(x, y) \tag{77}$$

and the force coefficients

$$Q_i = \sum_{j=1}^{J} b_j Q_{ij}, \tag{78}$$

where

$$Q_{ij} = \frac{s}{2D}\int_{-1}^{1}\int_{x_l(\eta)}^{x_t(\eta)} Z_i(x/d, \eta) l_j(x, \eta s)\, dx\, d\eta. \tag{79}$$

The basic modes Z_j fall into four categories according to their spanwise symmetry or antisymmetry and their analytical or numerical definition. The analytical 'standard modes' are selected from

$$Z = X^{\sigma} Y^{\tau}, \tag{80}$$

where $X = x/d$, $Y = \eta$ and the integers σ ($\geqslant 0$) and τ ($\geqslant 0$) satisfy $\sigma + \frac{1}{2}\tau \leqslant 4$; thus, fifteen symmetrical and ten antisymmetrical standard modes are available as indicated in Table II.1 of Appendix II. The numerical modes are defined by values of Z_j and $\partial Z_j/\partial X$ at the collocation points where equation (74) is to be evaluated. The weighting Z_i in equation (79) is determined for each collocation section as a polynomial in X of degree $(2N - 1)$ consistent with the local values of both Z_i and $\partial Z_i/\partial X$.

Spanwise symmetry is denoted by sym $= 1$, antisymmetry by sym $= -1$, and both together by sym $= 0$. Restrictions on the numbers of modes are discussed in Appendix II and are represented approximately in equations (II.5) to (II.7). If there are numerical modes when sym $= 0$, the parameter ζ is used to indicate how many of these are symmetric.

4.3. Choice of Parameters

Given the rounded planform data and mode data outlined in Sections 4.1 and 4.2, it is necessary to specify the subsonic Mach number M and frequency parameter $\bar{\nu}$ to complete the definition of the aerodynamic problem. The facility wing $= 4$ for planform data and the use of numerical modes together imply a prior choice of the parameters N, m and a, which should be as small as is compatible with the desired accuracy.

The number of chordwise terms is dictated primarily by the behaviour of the complex upwash $\bar{w}/U$ in equation (74). The higher the power σ in equation (80) and the higher the frequency parameter, the larger N needs to be. It is reasonable to take

$$N > 2 + \sigma + \frac{2\bar{\nu}}{\pi}, \tag{81}$$

but low aspect ratio or high sweepback or high M may call for a further increase. The number of collocation sections is governed primarily by the aspect ratio, but the demand is probably increased in cases of high sweepback or high taper or an increase in the power τ in equation (80). As a guide line we suggest

$$\left.\begin{aligned} m &\geqslant 10 \\ m &> \tau + \frac{4sc_R}{\bar{c}^2}\sec\Lambda_t \end{aligned}\right\} \tag{82}$$

where Λ_t is the sweepback of the trailing edge. The spanwise integration parameter must increase with the number of chordwise terms, lest the matrix elements $\Omega_q(p, \nu, r)$ in equation (24) should become inaccurate at the forward positions $p = 1$. If m is determined from the second inequality (82), then a satisfactory value of a is $(2N - 4)$; in general we suggest

$$a(m + 1) > (2N - 4)(1 + 2A). \tag{83}$$

This should provide roughly three-figure or $\pm\frac{1}{2}$ per cent accuracy in the generalised forces.

There are four other parameters to define the calculation of the basic matrix $\Omega_q(p, v, r)$ in equation (23). As stated in Appendix II, the values for routine operation are

$$\left.\begin{aligned} n_{\max} &= 2^{\delta} = 128, & \lambda_{\text{int}} &= 3 \\ \text{tol} &= 10^{-\varepsilon} = 10^{-4}, & \kappa &= 0{\cdot}5 \end{aligned}\right\}. \tag{84}$$

Refinement in accuracy is obtainable by taking $\delta > 7$ and $\varepsilon > 4$, but only with a considerable penalty in computing time according to equation (II.9).

4.4. Programs I and II

The preparation of data for the first stage of the program is summarised in Table II.2 and illustrated in Appendix III. The indicators 'stop' and 'print' are introduced to control the end of the computation and the output. The various options are included in Table II.4. The larger the value of stop, the more the computation is curtailed: the larger the value of print, the greater the output. In the normal calculation with stop = print = 0, the matrix of complex generalised force coefficients Q_{ij} is evaluated and printed out together with the input data, the required storage from equations (II.1) and (II.4), the solutions $(\Gamma_{qr})_j$ and the running time. With stop = print = 1, the computation does not proceed beyond the solutions $(\Gamma_{qr})_j$, while the matrix $\Omega_q(p, v, r)$ and right hand sides h_{pv} from equation (60) are printed as additional output. In matrix notation we write

$$[\Omega][\Gamma] = [h], \tag{85}$$

where $[\Omega]$ is the square influence matrix of order mN with element $\Omega_q(p, v, r)$ in row $\{(p-1)m + v\}$ and column $\{(q-1)m + r\}$ and in corresponding order $[\Gamma]$ and $[h]$ are column matrices with respective elements Γ_{qr} and h_{pv}. With stop = 2, print = 3, only the matrix is calculated, but it is output on paper tape as well as by line printer. Ten other combinations of stop and print appear in Table II.4, and the flow diagram in Figs. 1a and 1b shows the various methods of operation and safeguards.

The facility print = 3 provides the link between Program I and Program II which has two main uses. As explained in Table II.5, the output paper tape comprises definitive planform data and the matrix $\Omega_q(p, v, r)$ and forms input tape A, the major part of the data for Program II. With the option stop = 0, the force coefficients Q_{ij} are calculated for arbitrary modes; this offers a large saving in running time if additional or amended modes are necessary. With the option stop = 5, the computation proceeds further to obtain the complex loading at chordwise positions

$$x = x_l(\eta) + \tfrac{1}{2}c(\eta)\left(1 + \cos\frac{v\pi}{V}\right), \qquad v = 1, 2, \ldots (V-1) \tag{86}$$

where the integer V is arbitrary. The quantity $l(x, y)$ from equation (61) is evaluated at all sections $\eta = \eta_r$ and, if desired, at T additional sections $\eta = \eta_t$, for which the values of $x_l(\eta_t)$ and $c(\eta_t)$ must appear on the supplementary input tape B as listed in Table II.5. The functions $(K_{qr})_i$ from equation (63) with $\eta = \eta_r$ serve to calculate not only Q_{ij} but the local lift and moment both of which are output when stop = 5. From equations (61) and (63) the local lift coefficient is

$$(C_{Lr})_j = \int_0^{\pi} (l_r)_j \tfrac{1}{2}\sin\phi \, d\phi = \frac{4s}{\pi c_r}\sum_{q=1}^{N} (K_{qr})_1(\Gamma_{qr})_j, \tag{87}$$

where $i = 1$ denotes that $z_i = z_1 = -d$. Similarly with

$$z_i = -\frac{d}{c_r}(x - x_{lr}) = \left(\frac{d}{c_r}\right)z_2 - \left(\frac{x_{lr}}{c_r}\right)z_1 \tag{88}$$

where

$$z_1 = -d \quad \text{and} \quad z_2 = -x,$$

the local pitching moment coefficient about the leading edge is given by

$$-(C_{mr})_j = \frac{4s}{\pi c_r} \sum_{q=1}^{N} \left\{ \left(\frac{d}{c_r} \right) (K_{qr})_2 - \left(\frac{x_{lr}}{c_r} \right) (K_{qr})_1 \right\} (\Gamma_{qr})_j. \tag{89}$$

The general flow diagram is shown in Fig. 2. The running time is trivial by comparison with that of program I.

There are slight complications when sym = 0, but the instructions in Appendix II should suffice. There are also greater restrictions on storage in Program I when sym = 0, because it is necessary to store the regularised influence functions $R_q(p, v, \lambda)$. In cases outside the range of Table II.6b and within the range of Table II.6a it would be necessary to run the symmetrical and antisymmetrical calculations separately.

5. Calculated Examples

The present method has been applied to the four planforms in Fig. 3, which shows their origins of coordinates and indicates the scope of the calculations. The numerical planform data are listed in Table 1, where the representative length $d(= 1)$ and area D are defined for each wing.

The elliptical wing has been used for numerical checks in Section 5.1. and as the illustrative example in Appendix III. Like the elliptical wing, the tapered swept wing of aspect ratio 2 is selected from the examples in Ref. 11, where the results of several current methods are compared. Being a wing of high sweepback, it is a suitable case in which to study solutions with odd and even values of m, respectively with and without collocation points on the centre line (Section 5.2.). The low-aspect-ratio rectangular wing in Section 5.3. makes little demand on the parameter m, but it serves to study convergence with respect to N at moderate and at high frequency parameter. The final example in Section 5.4., a tapered swept wing of aspect ratio 6, has the most practical planform and provides a thorough examination of the present method at two Mach numbers and over a wide range of frequency.

5.1. Elliptical Wing

At the outset of the present investigation the method of Ref. 8 for steady flow was reformulated conveniently for the extension to oscillatory conditions. The case of a circular wing at $M = 0$ with $N = 3(R = 2), m = 5, a = 2$ in Table 2A of Ref. 8 furnished a good example on which to check the formulae by hand calculation, and the results were reproduced to all six decimal places. The computation involved non-zero values of the first and second derivatives of the planform geometry $x_l(\eta)$ and $c(\eta)$, which provided the necessary generality.

The main calculation to be completed on a desk machine was for an elliptical planform at Mach number $M = 0{\cdot}8$ and frequency parameter

$$k = \frac{\omega s}{U} = 1 \tag{90}$$

and of the same reduced aspect ratio βA as the circle. As a computational aid there was, fortunately, an established program for the influence functions F_q from equation (54), which had already been developed in connection with Ref. 3. The greatest difficulty in arriving at the complex matrix equation (85) concerned the computation of $R_q(p, v, \lambda)$ from equation (58) in the special cases $\lambda = av$. The limiting expression in steady flow from equations (38) to (41) is manageable enough, but for general frequency the quantity $D_q(p, v) \equiv D_q(X)$ in equation (I.23) of Appendix I requires special elaboration.

After the desk calculation for $N, m, a = 3, 5, 2$ had been completed, a first version of the present program became available; this test case, used as the illustrative example in Appendix III, confirmed numerical accuracy to the fourth decimal place, the small discrepancies being accepted in view of the large computing effort in evaluating $D_q(p, v)$ to improved accuracy by hand.

With reference to equations (81) to (83), it is reasonable to take $N = 4$, $m = 11$, $a = 6$ for simple modes of oscillation; instead of $(\delta, \varepsilon) = (7, 4)$ as in equation (84), the extra accuracy with $(\delta, \varepsilon) = (8, 6)$ is used in the solution quoted in Table 2. The force coefficients

$$Q_{ij} = Q'_{ij} + ikQ''_{ij} \tag{91}$$

for symmetric modes $Z = 1, X, X^2, Y^2$ and antisymmetric modes $Z = Y, XY$ agree with those of Ref. 11, to the order of accuracy, 1 or 2 per cent, revealed by those comparisons.

Since the planform has streamwise symmetry, we may apply the reverse-flow theorem as given by the identity in equation (19) of Ref. 12. Thus, from equations (32) of Ref. 12, we have the identity

$$Q_{12} + Q_{21} + \frac{iQ_{11}}{k} = 0 \tag{92}$$

without the term in c_R because the origin at the centre of the ellipse occurs in the transverse plane of symmetry. Similarly there is the identity

$$Q_{23} + Q_{32} + \frac{i}{k}(Q_{13} + 2Q_{22}) = 0, \tag{93}$$

where the modes 1, 2 and 3 correspond to $Z = 1$, X and X^2 respectively. With the aid of equation (91) the real and imaginary parts of equations (92) and (93) give

$$\left.\begin{aligned} Q'_{12} + Q'_{21} - Q''_{11} &= 0 \\ Q''_{12} + Q''_{21} + k^{-2}Q'_{11} &= 0 \\ Q'_{23} + Q'_{32} - Q''_{13} - 2Q''_{22} &= 0 \\ Q''_{23} + Q''_{32} + k^{-2}(Q'_{13} + 2Q'_{22}) &= 0 \end{aligned}\right\}. \tag{94}$$

The solutions in Table 2 with $k = 1$ give respective left hand sides 0·0002, 0·0004, 0·0004 and 0·0006, which are consistent with results correct to the third decimal place. The left hand sides of equations (94) have also been calculated for the other solutions in Ref. 11, and the next best set of values is 0·0000, 0·0021, 0·0009 and 0·0048 as found from Ref. 13; all the others show errors in the second decimal, possibly due to taking only three chordwise terms. The root-mean-square error between the 32 force coefficients in Table 2a and the corresponding values from Ref. 13 is 0·0062, while for the antisymmetrical modes in Table 2b it is only 0·0004; with reference to the value of Q''_{11}, the damping derivative in heave (or roll), the worst of the discrepancies is about $\frac{1}{2}$ per cent and of no practical concern.

5.2. Tapered Swept Wing (A = 2)

As shown in Fig. 3, the planform has high leading-edge sweepback. The choice of artificial central rounding is therefore a matter of importance, and we have used equations (67), (68) and (70) with

$$\eta_{iR} = \sin\left(\frac{\pi}{16}\right) = 0{\cdot}19509.$$

The reference length $d = s$, area $D = s^2$ and origin at mid-root-chord are taken in Table 1 to be consistent with Ref. 11, so as to facilitate comparisons with other methods; for the same reason the Mach number is

fixed at $M = 0{\cdot}7806$ ($\beta = 0{\cdot}625$) and the frequency parameter

$$k = \frac{\omega s}{U} = \frac{\omega \bar{c}}{U} = \bar{\nu} = 1. \tag{95}$$

For the simple rigid modes of heaving and pitching, equations (81) to (83) suggest that it is reasonable to take $N = 4, m = 14, a = 2$. Most of the present calculations have been made with $N = 3$ to correspond to the original results for this wing in Ref. 3 and most of those in Ref. 11. However, the calculated force coefficients $Q_{ij}(i, j = 1$ and $2)$ in Table 3a include one set obtained with $N = 4$.

The four solutions with $N = 3$ show the negligible effect of increasing (δ, ε) from (7, 4) to (8, 6) and of increasing a from 2 to 3. Moreover, the increase in m from 14 to 15 barely affects Q'_{ij} or Q''_{ij} in the third significant figure. Considering that this change in m produces full interspersion of collocation sections in the central region, we may fairly conclude that the artificial rounding is effective. By contrast, a problem of collocation error was encountered for the same planform at low frequency in Fig. 22 of Ref. 14 when the method of Ref. 6 was applied with insufficient rounding and therefore with excessive curvature of planform at the central collocation section. The procedures in Section 4.1. appear to avoid this difficulty.

The remaining solution with $N = 4$ shows much more effect of this parameter than any of the others, changes of up to 4 per cent being found in Table 3a when N is increased from 3 to the recommended value 4. Perhaps equation (81) is a little optimistic for such a high value of leading-edge sweep parameter as

$$\beta^{-1} \tan \Lambda_l = 2{\cdot}77.$$

Convergence with respect to N will be considered more fully for the remaining planforms in Sections 5.3. and 5.4.

Table 3b shows comparisons of the present results with those of Ref. 3 and others quoted in Ref. 11. Both Acum's[3] original calculations and those by Laschka's[15] method* with $N = 3$ and $m = 15$ are in satisfactory agreement with corresponding results by the present method; the worst differences of about 2 per cent are of the same order as the effect of increasing N from 3 to 4. The comparisons with $N = 4$ and m even ($\geqslant 14$) do not show the method of Ref. 13 in such a favourable light as the previous discussion for the elliptical wing. The differences average above 4 per cent, and the worst discrepancies (in Q'_{12} and Q'_{22}) may be written as $0{\cdot}023Q''_{11}$ by comparison with $0{\cdot}006Q''_{11}$ for the elliptical wing. The most likely explanation lies in the severe kink at the apex of the leading edge. Nevertheless the results by Long's[7] method with $N = 4$ are reasonably close to the corresponding values by the present method in view of differences in assumed central rounding and the incomplete convergence with respect to N. Whilst an increase in Mach number or frequency would aggravate the question of accuracy, none of the disparities in Table 3b is likely to discourage the use of the various methods in flutter calculations.

5.3. Rectangular Wing (A = 1·25)

The rectangular wing is of such small aspect ratio $A = 1{\cdot}25$ that $m = 11$ is sure to suffice. We can therefore concentrate on the other parameters N, a, δ and ε at the moderate and high frequency parameters $\bar{\nu} = 1{\cdot}5$ and $6{\cdot}0$ in incompressible flow. The generalised forces in Table 4 correspond to the modes of heaving and pitching about the leading edge.

Consider first the parameters δ and ε introduced in equation (84). Before the computer program was optimised, the maximum number of intervals in the integration routine for the influence functions was often fixed at 2^δ with $\delta = 8$ or 9; moreover the tolerance $10^{-\varepsilon}$ was usually selected with $\varepsilon = 6$ or more. With the recommended values $(\delta, \varepsilon) = (7, 4)$, the influence matrix $[\Omega]$ shows small inaccuracies in its elements, but the equations are so well-conditioned that there are virtually no discrepancies in the final calculation of generalised forces. Table 4 shows that at both frequencies the changes in Q'_{ij} and Q''_{ij} are insignificant to the fourth decimal place when δ is increased to 8 and then ε is increased to 6. This same

* Results are given in V.F.W. Report M-75/66 (B. Laschka, G. Böhm, H. Schmid, 1966).

negligible effect was found for the two previous wings and appears to be irrespective of Mach number and frequency parameter. The facility to vary (δ, ε) appears to have served its purpose by more than halving the running time as estimated in equation (II.9) of Appendix II.

Equation (81) suggests that $N = 4$ and $N = 7$ should suffice when $\bar{\nu} = 1{\cdot}5$ and $6{\cdot}0$ respectively, and with $m = 11$ the respective values $a = 2$ and $a = 3$ or 4 are recommended in equation (83). The calculated generalised forces in Table 4 show slight changes in the fourth significant figure when a is increased from 4 to 6 and $N = 4$. This is so small compared with the alarming effect of N when $\bar{\nu} = 6{\cdot}0$, that $a = 4$ is retained in the study of convergence with respect to N. This aspect of the results is illustrated in Figs. 4 and 5 by parabolic curves of pitching stiffness and damping against axis position, viz.,

$$Q_{22}\left(\frac{x_0}{\bar{c}}\right) = Q'_{22}\left(\frac{x_0}{\bar{c}}\right) + i\bar{\nu}Q''_{22}\left(\frac{x_0}{\bar{c}}\right)$$

$$= Q_{22}(0) - \frac{x_0}{\bar{c}}[Q_{12}(0) + Q_{21}(0)] + \left(\frac{x_0}{\bar{c}}\right)^2 Q_{11}(0). \tag{96}$$

The curves for $N = 3$, 4, 5 and 6 become progressively closer until those for $N = 6$ and $N = 7$ would differ by no more than the thickness of a line. It is of passing interest that the threat of negative pitching damping, predicted in Fig. 5 with $N \leqslant 5$, is dispelled by the more accurate calculations. The particular derivatives Q'_{22} and Q''_{22} for the quarter-chord pitching axis are plotted against N in Fig. 6. Whilst $N = 4$ appears to be more than adequate for the lower frequency parameter $\bar{\nu} = 1{\cdot}5$, one needs to go to $N = 7$ or above to obtain comparable accuracy when $\bar{\nu} = 6{\cdot}0$.

A further illustration of convergence follows from reverse-flow checks similar to those in Section 5.1. Since the y-axis on the leading edge is no longer an axis of symmetry and is therefore displaced unit distance in the reverse flow, the first two of equations (94) now become

$$Q'_{12} + Q'_{21} - Q'_{11} - Q''_{11} = 0 \tag{97}$$

and

$$Q''_{12} + Q''_{21} - Q''_{11} + \frac{Q'_{11}}{\bar{\nu}^2} = 0. \tag{98}$$

The left hand sides are calculated from the present solutions in the following table.

$\bar{\nu}$	N	a	Eqn. (97)	Eqn. (98)
1·5	3	6	0·0004	0·0006
	4	6	0·0001	0·0001
	5	6	0·0000	0·0000
6·0	4	4	0·1053	0·0156
	5	4	0·0208	0·0021
	6	4	0·0061	0·0002
	7	4	0·0046	−0·0001

While the results are wholly satisfactory for $\bar{\nu} = 1{\cdot}5$, those for $\bar{\nu} = 6{\cdot}0$ show a convincing improvement as N increases.

By application of the reverse-flow theorem, the present solutions have been used to obtain the lift and pitching moment arising from an oscillating control surface, as recently reported by Drane and

Destuynder[16]. The range of frequency parameter in the associated experiments was particularly large, and the corresponding theoretical calculations have accentuated the need to increase the number of chordwise terms if convergence is to be maintained. It is with $N > 4$ that the facility to increase the parameter a becomes crucial to accuracy in the influence matrix, and more especially in the following Section 5.4. when the aspect ratio is no longer small.

5.4. Tapered Swept Wing (A = 6)

The fourth planform in Fig. 3 has been selected as being typical of designs for high subsonic cruise. In all the solutions to be considered, including those by the method of Ref. 7, the central rounding is defined by equations (67), (68) and (70) with $\eta_{iR} = 0{\cdot}19509$. The calculations for $M = 0{\cdot}4$ and $0{\cdot}8$ cover the wide range of frequency parameter $0 < \bar{\nu} \leqslant 4{\cdot}345$. The corresponding range of N from equation (81) is $4 \leqslant N \leqslant 6$, while equations (82) and (83) suggest $m = 19$ and $3 \leqslant a \leqslant 6$. Most of the calculations use $N, m, a = 6, 15, 4$, but the results in Tables 5, 6 and 7 include variations of each parameter.

The convergence with respect to N has only been studied in the worst case with the largest values of $M = 0{\cdot}8$ and $\bar{\nu} = 4{\cdot}345$. In Fig. 7, the cross derivatives $Q'_{12}, Q'_{21}, Q''_{12}$ and Q''_{21} are plotted against N ($4 \leqslant N \leqslant 7$). Although the presentation is less consistent than for the rectangular wing in Fig. 6, it suggests that accuracy to three significant figures has been approached, apart from the smallest coefficient Q'_{12}. The effect of increasing the spanwise integration parameter from $a = 4$ to $a = 6$ is also of order 0·01 and small enough to encourage confidence that the extreme combination of Mach number and frequency parameter can be handled satisfactorily.

Figs. 8 to 10 concern the effect of frequency, which is expected to be large when the aspect ratio is large. The stiffness derivatives $Q'_{11}, Q'_{12}, Q'_{21}$ and Q'_{22} for $M = 0{\cdot}8$ in Fig. 8 all change sign in the range $0 < \bar{\nu} < 5$, but their behaviour in the upper part of the range is reasonably consistent with the trend set in the lower part. By contrast, still at $M = 0{\cdot}8$, the corresponding curves of damping derivatives in Fig. 9 do not involve any change of sign, but have unexpected points of inflexion near $\bar{\nu} = 3$. The direct pitching damping Q''_{22} has such a marked increase in slope in the region $\bar{\nu} > 3$, that the question of reliability is raised, although it would appear from the evidence in Table 6 that the effect is genuine. The trends with frequency parameter are intensified at the lower Mach number $M = 0{\cdot}4$, as illustrated for Q'_{22} and Q''_{22} in Fig. 10. The stiffness derivative shows the usual smallish compressibility effect at $\bar{\nu} = 0$, but it changes sign at much smaller $\bar{\nu}$ when $M = 0{\cdot}4$ and soon reaches negative values of much greater magnitude than the static value. The behaviour of the damping derivative in Fig. 10 can be made to appear quite logical. The initial slopes are known from equation (17) of Ref. 17, viz.,

$$\left(\frac{\partial Q''_{ij}}{\partial \bar{\nu}}\right)_{\bar{\nu}\to 0} = \frac{1}{16} A(Q'_{1j}Q'_{i2})_{\bar{\nu}\to 0}$$

$$= 2{\cdot}077 \text{ and } 3{\cdot}107 \text{ when } i = j = 2 \tag{99}$$

for $M = 0{\cdot}4$ and $0{\cdot}8$ respectively. These initial slopes, indicated by broken lines, are not maintained for long and, as is usual, the rates of change of Q''_{22} with respect to $\bar{\nu}$ soon become relatively small. However, the required limit from piston theory, which becomes exact as $\bar{\nu} \to \infty$, requires that

$$Q_{22} = \frac{2}{MS}\int_S\int \frac{x - x_0}{\bar{c}}\left[1 + \frac{i\bar{\nu}(x - x_0)}{\bar{c}}\right] dx\, dy. \tag{100}$$

From equation (100) and the definition of the planform in Table 1, it may be shown that

$$(Q'_{22})_{\bar{\nu}\to\infty} = \frac{2}{M}\left(1{\cdot}4717 - \frac{x_0}{\bar{c}}\right) \tag{101}$$

and

$$(Q''_{22})_{\bar{\nu}\to\infty} = \frac{2}{M}\left[2{\cdot}4992 - 2{\cdot}9434\frac{x_0}{\bar{c}} + \left(\frac{x_0}{\bar{c}}\right)^2\right] \tag{102}$$

$$= 12{\cdot}496 \text{ and } 6{\cdot}248 \text{ when } x_0 = 0$$

for $M = 0{\cdot}4$ and $0{\cdot}8$ respectively. A dramatic increase in $\partial Q''_{22}/\partial\bar{\nu}$ is required when $M = 0{\cdot}4$; although much more gentle, the same trend is found necessary at $M = 0{\cdot}8$. Without these explanations the double cross-over of the two curves in Fig. 10 might appear unrealistic.

The influence of axis position on pitching damping is illustrated in the two remaining diagrams. In Fig. 11, the curves of Q''_{22} from the imaginary part of equation (96) for $M = 0{\cdot}8$ and selected values $\bar{\nu} = 0, 0{\cdot}5$, $1{\cdot}608$ and $3{\cdot}157$ shown an initial shift in the axis position for minimum damping from $x_0 = 1{\cdot}06\bar{c}$ when $\bar{\nu}$ is very small to above $x_0 = 1{\cdot}45\bar{c}$ when $\bar{\nu} > 1$. The limit from equation (102), plotted as a broken curve, indicates what might be expected above $\bar{\nu} = 3{\cdot}157$. Indeed, the calculated minimum when $\bar{\nu} = 4{\cdot}345$, i.e., $Q''_{22} = 0{\cdot}674$, is about as small as its theoretical value for this wing can be when $M = 0{\cdot}8$. Fig. 12 shows a substantial reduction in the minimum when $M = 0{\cdot}4$, though there is no danger of negative damping.

The relationships in equations (32) of Ref. 12 have been used to obtain numerical values of Q'_{ij} and Q''_{ij} from solutions for the complex generalised forces $\bar{Q}_{ij}$ on the reversed planform with leading and trailing edges interchanged. For $M = 0{\cdot}4$, two such sets of results are included in Table 5; thus we calculate the reverse-flow curve $Q''_{22}(x_0/\bar{c})$ of short dashes in Fig. 12 with $N, m, a = 6, 15, 6$ to compare with the full curve from the corresponding direct solution. While the two curves are not in serious disagreement, the difference between them suggests that convergence with respect to m may not be complete. Whereas for the tapered swept wing of lower aspect ratio in Table 3 there was only a small effect of changing m from 15 to 14, the corresponding results for $A = 6$ in Table 5 show differences of the same order as those revealed by the reverse-flow check. The comparative exercise has therefore been repeated with $m = 22$ and 23 and a reverse-flow check in the latter case. The discrepancies are significantly reduced and never exceed $0{\cdot}05Q''_{11}$ as compared with $0{\cdot}13Q''_{11}$ with the two smaller values of m. While it is not possible to state with any certainty that even values of m are preferable on wings of high sweepback, there is a remarkable agreement in Table 5 between the direct 6, 22, 4 solution and reverse-flow result with $N, m, a = 6, 23, 4$.

The final comparisons are between the present solutions and those by the method of Ref. 7 with $m = 14$, $N = 6$ and variation of the spanwise integration parameter, denoted by q in Ref. 7. There can be little doubt that the two methods would yield identical results if, respectively, a and q were increased indefinitely. Table 7 shows a tendency, which has also been noted from downwash studies in Fig. 3 of Ref. 18, that convergence with respect to both a and q involves a maximum in the error prior to eventual convergence. The result by the method of Ref. 7 with $q = 1$ is virtually what would be expected by Davies'[4] method. On each derivative the result for $q = 5$ has overcorrected the initial integration error. As q increases to 9, the error begins to subside towards the present result, which is only slightly altered by the change from $a = 6$ to $a = 10$ and converges from the opposite direction; moreover, the $q = 9$ solution differs from the converged result by no more than the residual discrepancies in Table 5 from considerations of m and N.

A fair conclusion from Fig. 3 of Ref. 18 is that the present method, developed from Ref. 8, and the method of Ref. 7, developed from Ref. 6, with $q = 2a$ are likely to yield similar accuracy for unswept wings at any rate. However, the outstanding advantage of the present method lies in the economy of computation, as emphasized at the foot of Table 7. Although Ref. 7 is particularly rapid when $q = 1$, the running time of the present method only grows in proportion to $a^{\frac{1}{2}}$ over the usual range $a \leqslant 8$, in accord with equation (II.8) and as a result of the efficient use of machine code.

6. Conclusions

(1) A linear theoretical method is formulated for general subsonic Mach number and frequency and for planforms with smooth leading and trailing edges in arbitrary modes of deformation. Procedures are incorporated for treating wings with several cranks by selected artificial rounding (Section 4.1.);

alternatively the planform may be defined numerically by leading edge and chord data including their first and second derivatives.

(2) The method is programmed in two parts, the first of which expresses the wing loading for each mode in terms of a set of complex numbers and provides a matrix of generalised force coefficients. Program I has a facility for outputting the aerodynamic influence matrix on tape, which is input into Program II to obtain generalized forces for additional modes and, if required, the load distributions at arbitrary sections.

(3) The program can be run for zero or very small frequency parameter, say $\bar{\nu} = 0{\cdot}0001$. Because it is based on a highly satisfactory method for steady flow and on the efficient KDF9 machine code, it is quicker and more accurate than the Algol program of Ref. 6 used previously.

(4) The restrictions on size of solution are indicated in Table II.6a, and the usable range of parameters should serve most needs. The requirement to handle wings of high aspect ratio demands quite large numbers of spanwise terms (Section 4.3.); moreover, the requirement to treat high values of the frequency parameter is shown to demand at least seven chordwise terms as compared with the four that are available in Ref. 6.

(5) Accuracy has been established by direct comparison with the limiting case of Ref. 8 when $\bar{\nu} = 0$, by hand calculation, by reverse-flow relationships, by asymptotic expansion for small frequency, and by studies of convergence. Results have been compared with those of other collocation methods in current use.

(6) Illustrative results for a tapered swept wing of aspect ratio 6 show larger frequency effects in the flutter range at low than at high subsonic Mach number. Because of its capability in the upper frequency range, the method is of considerable potential in relation to non-harmonic time-dependent flows where linear theory is applicable, in particular to the growth of lift as a wing enters a gust.

Acknowledgements

The programming in KDF9 Usercode was carried out by Mr. P. S. Hampton under the supervision of Mr. A. R. Curtis in the Division of Numerical and Applied Mathematics, N.P.L. Acknowledgements are made to the KDF9 machine operators of the Central Computer Unit, N.P.L. Special credit is due to Mrs. Sylvia Lucas, who handled the exacting desk calculations with exemplary precision and assisted in the preparation of tables and illustrations. Mrs. Sandra Inch was responsible for most of the data tapes. The authors also wish to acknowledge helpful discussions with Mr. W. E. A. Acum of Ship Division, N.P.L., and the co-operation of Mr. D. L. Woodcock and Dr. D. E. Davies of Structures Department, R.A.E., and Mr. G. Long of the Aeronautical Research Laboratories, Australia in providing numerical data by other methods.

LIST OF SYMBOLS

a	Factor controlling number of spanwise integration points
a_q, b_q	Coefficients in equation (I.21)
A	Aspect ratio of planform; $2s/\bar{c}$
b_j	Coefficient of downwash mode in equation (76)
$c(\eta)$	Local chord
$\bar{c}$	Geometric mean chord; $S/2s$
c_v, c'_v, c''_v	$c(\eta)$ and its first two derivatives at $\eta = \eta_v$
C_L	Lift coefficient; lift/$(\frac{1}{2}\rho U^2 S)$ in equation (48)
$(C_{Lr})_j$	Local lift/$(\frac{1}{2}\rho U^2 c_r)$ at $\eta = \eta_r$ in equation (87)
C_m	Nose-up pitching moment/$(\frac{1}{2}\rho U^2 Sd)$ about y-axis in equation (49)
$(C_{mr})_j$	Local pitching moment/$(\frac{1}{2}\rho U^2 c_r^2)$ about leading edge in equation (89)
d	Representative length (usually s or $\bar{c}$)
D	Representative area (usually s^2 or S)
$D_q(X)$	Function in equation (33) or (I.23); also written as $D_q(p, v)$
$E_q(X)$	Function in equation (32) or (55); also written as $E_q(p, v)$
$f(\lambda)$	Shape of artificial rounding; $f_1(\lambda)$ or $f_2(\lambda)$ in equations (66)
$F_q(p, v, \lambda)$	Influence function in equation (8) or (I.1)
$g(\lambda)$	Artificial rounding function; $g_1(\lambda)$ or $g_2(\lambda)$ in equation (68) or (69)
$G_1, \ldots G_4$	Contributions to kernel function in equation (I.1) and defined in Ref. 3
$(h_{pv})_j$	Element of right hand side of equation (85); $-\bar{w}_j/U$
i	$\sqrt{-1}$ or integer denoting force mode, e.g., lift ($i = 1$), pitching moment ($i = 2$)
I	Alternative integrals in equations (I.21) and (I.23)
j	Integer ($\leqslant J$) denoting downwash mode, e.g,, heaving ($j = 1$), pitching ($j = 2$)
$J(\eta'), J'(\eta')$	Function in equation (36) and its derivative; see also equations (41)
k	Frequency parameter $\omega d/U$
K	Kernel function in equation (2); *see* also equation (27) of Ref. 3
$(K_{qr})_i$	Integrated chordwise loading in equations (63) and (64)
$l(x', y')$	Lift per unit area/$(\frac{1}{2}\rho U^2)$ in equation (3)
ln	Natural logarithm (to base e)
$\bar{l}$	Modified complex loading in equations (51)
$(l_r)_j$	Complex loading at section $\eta = \eta_r$ in downwash mode j
$L_q(X)$	Chordwise integral with first and second derivatives $L'_q(X)$ and $L''_q(X)$ in equations (29) to (32)
m	Number of collocation sections
m^*	$\frac{1}{2}m$ or $\frac{1}{2}(m + 1)$ according as m is even or odd
M	Mach number of stream
$n_{\max}$	Maximum number of intervals in evaluating the integral F_q
N	Number of chordwise functions or collocation points
p	Integer 1(1)N denoting chordwise positions $x = x_{pv}$
P_1, P_2, P_3	Functions in equations (I.7), (I.8), (I.9)
$P_q(x, \eta; \eta')$	Modified influence function in equation (9) also written as $P_q(p, v, \lambda)$

P'_q, P''_q	$\partial P_q/\partial\eta'$, $\partial^2 P_q/\partial\eta'^2$ in equations (35), (37) respectively
q	Integer 1(1)N denoting particular function $\Psi_q(\phi')$
q	Factor in Ref. 7 (analogous to a)
Q_i	Force/$\rho U^2 D$ in mode z_i in equation (75)
Q_{ij}	Generalised force coefficient in force mode i and downwash mode j
Q'_{ij}, Q''_{ij}	Stiffness and damping coefficients; $Q_{ij} = Q'_{ij} + ikQ''_{ij}$
r	Integer 1(1)m denoting loading station $\eta = \eta_r$
R	Quantity in equation (II.2)
$R_q(x, \eta; \eta')$	Regularised influence function in equations (13) or (40)
s	Semi-span of wing
S	Area of planform
t	Time
$\bar{t}$	X or $(1 - X)$, whichever is the smaller
T	Number of Sections $\eta = \eta_t$
T_1, T_2, T_3	Functions in equations (I.16), (I.17), (I.18)
U	Velocity of stream
v, V	Integers in equation (86) for chordwise loading positions
$w(x, y)$	Upwash velocity in equation (1); see also equation (59)
$\bar{w}$	Modified complex upwash in equation (50)
x	Ordinate in streamwise direction (Fig. 3)
x'	Streamwise variable in downwash integral
x_0	Location of pitching axis; usually $x_0 = 0$, but see equation (96)
$x_l(\eta)$	Ordinate of leading edge
x'_{lv}, x''_{lv}	First and second derivatives of $x_l(\eta)$ at $\eta = \eta_v$
x_{pv}	Ordinate of collocation point in equation (17)
$x_t(\eta)$	Ordinate of trailing edge
X	Influence function parameter in equation (7); otherwise x/d or x/c
X_0, X_p	Chordwise variables $\frac{1}{2}(1 - \cos\phi)$, $\frac{1}{2}(1 - \cos\phi_p)$
y	Ordinate in standard direction (Fig. 3)
y'	Spanwise variable in downwash integral
y_v	Location of collocation section; $-s\cos\left(\dfrac{v\pi}{m+1}\right)$
Y	Influence function parameter in equation (7); otherwise y/s
$\bar{Y}$	Supplementary variable in equation (I.7)
z	Ordinate in upward direction
z_i, z_j	Modes $z(x, y)$ corresponding to i, j
Z_i, Z_j	Non-dimensional mode $-z/d = Z(x/d, y/s)$, e.g., equation (80)
Z_{num}	Non-standard mode defined by numerical values of Z_{pv} and Z'_{pv}
Z_{pv}, Z'_{pv}	Values of Z and $\dfrac{\partial Z}{\partial(x/d)}$ at collocation point (x_{pv}, y_v)

β	Compressibility factor; $(1 - M^2)^{\frac{1}{2}}$
$\Gamma_q(\eta')$	Spanwise loading function in equations (3) and (11)
$(\Gamma_{qr})_j$	Loading coefficient in mode j; element of unknown column matrix in equation (85)
δ	Accuracy parameter given by $n_{\max} = 2^{\delta}$
ε	Accuracy parameter given by $\text{tol} = 10^{-\varepsilon}$
ζ	Number of symmetric modes Z_{num} when sym = 0
η, η'	Spanwise ordinates y/s, y'/s
η_i, η_{iR}	Extent of artificial rounding, e.g., $\lvert\eta\rvert \leqslant \eta_{iR}$ for central crank
η_r	Loading station $\eta = -\cos\left(\dfrac{r\pi}{m+1}\right)$
η_t	Section $\eta(\neq \eta_v)$ where loading is to be calculated
η_λ	Spanwise integration point where $\eta = -\cos\left(\dfrac{\lambda\pi}{\Lambda+1}\right)$
η_v	Collocation section $\eta = -\cos\left(\dfrac{v\pi}{m+1}\right)$
θ', θ_v	Angular spanwise parameters $\cos^{-1}(-\eta')$, $v\pi/(m+1)$
κ	Parameter for subdividing chordwise integration $(=\frac{1}{2})$
$\kappa_{r\lambda}$	Coefficient in equation (19)
λ	Integer 1(1)Λ in spanwise integration of downwash
λ, λ_K	Artificial rounding parameter, $\lvert\eta - \eta_K\rvert/\eta_{iK}$ for crank at $\eta = \eta_K$
λ_{int}	Number of terms used in estimating convergence of spanwise integration $(=3)$
Λ	Number of spanwise integration points; $a(m+1) - 1$
Λ^*	$\frac{1}{2}\Lambda$ or $\frac{1}{2}(\Lambda + 1)$ according as Λ is even or odd
$\Lambda_l, \Lambda_{\frac{1}{2}}, \Lambda_t$	Angles of sweepback of leading edge, midchord, trailing edge
μ, μ_v	Local frequency parameters $\omega c(\eta')/(\beta^2 U)$, $\omega c_v/(\beta^2 U)$
ν	Integer 1(1)m denoting collocation section $\eta = \eta_v$
$\bar{\nu}$	Frequency parameter $\omega\bar{c}/U$
ξ	Chordwise variable equivalent to X_0
ρ	Density of stream
ρ_{vr}	Coefficient in equation (20)
σ, τ	Indices in equation (80)
σ, τ	Parameters for running time in equations (II.8) and (II.9)
σ_{vr}	Coefficient in equation (21)
Σ	Word storage; Σ_{I} or Σ_{II} in equations (II.1) or (II.3)
τ_{vr}	Coefficient in equation (22)
ϕ, ϕ'	Angular chordwise parameters in equations (29), (5)
ϕ_p	$2\pi p/(2N+1)$; values of ϕ at collocation point
$\Psi_q(\phi')$	Chordwise loading function in equation (4)
ω	Circular frequency of oscillation
$\Omega_q(p, v, r)$	Element of aerodynamic influence matrix in equations (24) and (85)
$A, -A$	Subscripts denoting cranks at $\eta = \eta_A, \eta = -\eta_A$ (wing = 3)
B	Subscript denoting crank at $\eta = \eta_B$ (wing = 3)

i	Subscript numerating force mode
j	Subscript numerating downwash mode
$K, -K$	Subscripts denoting cranks at $\eta = \eta_K, \eta = -\eta_K$ (wing = 2)
l	Subscript denoting leading edge
p	Subscript numerating chordwise collocation point
q	Subscript numerating chordwise loading function
r	Subscript numerating spanwise loading station $\eta = \eta_r$
R	Subscript denoting root section or central crank
t	Subscript denoting trailing edge
t	Subscript denoting optional section $\eta = \eta_t$ where load is calculated
T	Subscript denoting tip section
λ	Subscript numerating spanwise integration point $\eta = \eta_\lambda$
v	Subscript numerating spanwise collocation point
print	Parameter to define output (Table II.4)
round	Parameter to define artificial rounding (Table II.1)
stop	Parameter to define extent of calculation (Table II.4)
sym	Parameter to define spanwise symmetry (Tables II.1, II.2)
tol	Parameter ($= 10^{-\varepsilon}$) to regulate accuracy of calculation
wing	Parameter to specify type of planform (Tables II.1, II.2)

REFERENCES

No.	Author(s)	Title, etc.
1	H. Multhopp	Methods for calculating the lift distribution of wings. (Subsonic lifting-surface theory). A.R.C. R. & M. 2884, 1950.
2	H. C. Garner	Multhopp's subsonic lifting-surface theory of wings in slow pitching oscillations. A.R.C. R. & M. 2885, 1952.
3	W. E. A. Acum	Theory of lifting surfaces oscillating at general frequencies in a subsonic stream. A.R.C. R. & M. 3557, 1959.
4	D. E. Davies	Calculation of unsteady generalised airforces on a thin wing oscillating harmonically in subsonic flow. A.R.C. R. & M. 3409, 1963.
5	C. E. Watkins, H. L. Runyan and D. S. Woolston	On the kernel function of the integral equation relating the lift and downwash distributions of oscillating finite wings in subsonic flow. N.A.C.A. Report 1234, 1955.
6	H. C. Garner and D. A. Fox	Algol 60 programme for Multhopp's low-frequency subsonic lifting-surface theory. A.R.C. R. & M. 3517, 1966.
7	G. Long	An improved method for calculating generalised airforces on oscillating wings in subsonic flow. A.R.C. R. & M. 3657, 1969.
8	P. J. Zandbergen, T. E. Labrujere and J. G. Wouters	A new approach to the numerical solution of the equation of subsonic lifting surface theory. N.L.R. Report T.R. G. 49, 1967.
9	B. L. Hewitt and W. Kellaway	A new treatment of the subsonic lifting surface problem using curvilinear co-ordinates. Part I—Details of the method as applied to regular surfaces with finite tip chords and a preliminary set of numerical results. B.A.C. Preston Division Report Ae. 290 (S. & T. Memo 20/68), 1968.
10	H. C. Garner, B. L. Hewitt and T. E. Labrujere	Comparison of three methods for the evaluation of subsonic lifting-surface theory. A.R.C. R. & M. 3597, 1968.
11	D. L. Woodcock	A comparison of methods used in lifting surface theory. A.G.A.R.D. Report 583, 1971.
12	D. E. Lehrian and H. C. Garner	Comparative numerical applications of the reverse-flow theorem to oscillating wings and control surfaces. A.R.C. R. & M. 3488, 1965.

No.	Author(s)	Title, etc.
13	W. S. Rowe	Collocation method for calculating the aerodynamic pressure distributions on a lifting surface oscillating in subsonic compressible flow. A.I.A.A. Symposium on Structural Dynamics and Aeroelasticity, Boston, 1965.
14	H. C. Garner	Numerical appraisal of Multhopp's low-frequency subsonic lifting-surface theory. A.R.C. R. & M. 3634, 1968.
15	B. Laschka	Zur Theorie der harmonisch schwingenden tragenden Fläche bei Unterschallanströmung. *Z. Flugwiss.*, Vol. 11, pp. 265–292, 1963.
16	D. A. Drane and R. Destuynder	Measurements in low speed flow of unsteady pressure distributions on a rectangular wing with an oscillating control surface. R.A.E. Technical Report 70182, A.R.C. 33080, 1970.
17	H. C. Garner and R. D. Milne	Asymptotic expansion for transient forces from quasi-steady subsonic wing theory. *The Aeronautical Quarterly*, Vol. XVII, pp. 343–350, 1966.
18	H. C. Garner and G. F. Miller	Analytical and numerical studies of downwash over rectangular planforms. *The Aeronautical Quarterly*, Vol. XXIII, pp. 169–180, 1972.
19	C. W. Clenshaw and A. R. Curtis ..	A method for numerical integration on an automatic computer. *Numerische Mathematik*, Vol. 2, pp. 197–205, 1960.
20	G. N. Watson	Theory of Bessel Functions. Second edition, Cambridge University Press, 1948.
21		English Electric Leo KDF9 Programming Mini-manual.
22		English Electric Leo-Marconi KDF9 Service. Routine Library Manual, Volume 4.

APPENDIX I

Evaluation of the Influence Functions and their Behaviour at Small Spanwise Distances

By A. R. Curtis and W. E. A. Acum

A convenient form for the influence function F_q is given in equation (114) of Ref. 3, namely

$$F_q = \int_0^1 [G_1 + G_2 + G_3 + G_4] f_q(X_0)\, dX_0, \tag{I.1}$$

where

$$f_q(X_0) = \frac{1}{\pi} X_0^{-\frac{1}{2}}(1 - X_0)^{-\frac{1}{2}}[\cos\{q - 1)\cos^{-1}(1 - 2X_0)\} + \cos\{q\cos^{-1}(1 - 2X_0)\}] \tag{I.2}$$

and the functions G_1, G_2, G_3 and G_4 are defined by equations (78)* to (82) of Ref. 3 and can readily be expressed in terms of

$$X_0 = \tfrac{1}{2}(1 - \cos\phi), M, \bar{v}, \frac{c(\eta')}{\bar{c}}, X \text{ and } Y.$$

The quantities

$$\bar{F}_q = \frac{1}{\pi}\int_0^\pi (G_1 + G_2 + G_3 + G_4)\cos q\phi\, d\phi \tag{I.3}$$

are introduced, so that

$$F_q = \bar{F}_{q-1} + \bar{F}_q, \qquad q = 1, 2, 3, \ldots. \tag{I.4}$$

It is possible so to arrange the formulae that only single quadratures of non-singular integrands over finite ranges are necessary, and for such quadratures the method of Chebyshev integration due to Clenshaw and Curtis[19] was chosen, since it offered economy in the number of evaluations of integrands. However many of the integrals can be expressed in the form

$$\bar{I} = \int_0^\pi f(\cos\phi)\cos r\phi\, d\phi \tag{I.5}$$

and may be approximated accurately and economically by

$$\bar{I}_n = \frac{\pi}{n}\sum_{s=0}^{n}{}'' f\left(\cos\frac{s\pi}{n}\right)\cos\frac{rs\pi}{n}, \tag{I.6}$$

the dashes denoting the inclusion of a factor $\frac{1}{2}$ for $s = 0$ and n. After some preliminary transformations,

* The exponential in equation (78) of Ref. 3 should read $\exp(-iM\bar{Y}/\beta)$, where $\bar{Y} = \bar{v}c(\eta')Y/\beta\bar{c}$.

and $\gamma = 0{\cdot}57721566$ is Euler's constant. The remaining part of D_q is the coefficient of Y^2 in

$$\int_0^1 (G_3 + G_4) f_q(X_0)\, dX_0 = L_q(1)[G_3 + G_4]_{X_0=1} - \int_0^1 L_q(X_0) \frac{\partial}{\partial X_0}[G_3 + G_4]\, dX_0$$
$$= T_1 + T_2 + T_3, \tag{I.15}$$

where

$$T_1 = \frac{L_q(1)}{M}\left[1 - \frac{M(1-X)}{\{(1-X)^2 + Y^2\}^{\frac{1}{2}}}\right] \exp\{-i\mu(1 - X + M[(1-X)^2 + Y^2]^{\frac{1}{2}})\} \tag{I.16}$$

$$T_2 = \frac{i\mu\beta^2 L_q(1)}{M} \int_0^{1-X} \exp\{-i\mu[v + M(v^2 + Y^2)^{\frac{1}{2}}]\}\, dv \tag{I.17}$$

and

$$T_3 = \int_0^1 L_q(X_0)\left[\frac{Y^2}{\{(X - X_0)^2 + Y^2\}^{\frac{1}{2}}} + \frac{i\mu M Y^2}{(X - X_0)^2 + Y^2}\right]$$
$$\times \exp\{i\mu(X - X_0 - M[(X - X_0)^2 + Y^2]^{\frac{1}{2}})\}\, dX_0. \tag{I.18}$$

The coefficient of Y^2 in T_1

$$= \tfrac{1}{2} L_q(1)\left[\frac{1}{(1-X)^2} - \frac{i\mu(1-M)}{1-X}\right] \exp\{-i\mu(1+M)(1-X)\} \tag{I.19}$$

from a direct Taylor expansion of equation (I.16). The contribution from equation (I.17) is obtained by expansion of the exponential and use of the result that the coefficient of Y^2 in the integral

$$\int_0^{1-X} [v + M(v^2 + Y^2)^{\frac{1}{2}}]^r\, dv$$

is

$$\left.\begin{array}{ll} 0 & (r = 0) \\ \frac{1}{2}M \ln(2 - 2X) + \frac{1}{4}M & (r = 1) \\ \dfrac{rM}{2(r-1)}(1+M)r^{-1}(1-X)^{r-1} & (r = 2) \end{array}\right\}.$$

The coefficient of Y^2 in T_2 is therefore

$$\tfrac{1}{2}i\mu\beta^2 L_q(1)\left[-i\mu\{\ln(2 - 2X) + \tfrac{1}{2}\} + \sum_{r=2}^{\infty} \frac{(-i\mu)^r(1+M)^{r-1}(1-X)^{r-1}}{(r-1)(r-1)!}\right]$$
$$= \tfrac{1}{2}\mu^2\beta^2 L_q(1)\left[\ln(2 - 2X) + \tfrac{1}{2} + \int_0^{\mu(1+M)(1-X)} v^{-1}(e^{-iv} - 1)\, dv\right]. \tag{I.20}$$

Although the term T_3 in equation (I.18) conveniently contains the factor Y^2, one cannot obtain the required coefficient of Y^2 by removing the factor and setting $Y = 0$. In order to extract the terms that

are $O(1)$ and $O(Y^2 \ln Y)$, it is necessary to split and rearrange the integration such that

$$
\begin{aligned}
T_3 = {} & Y^2 \int_0^{\bar{t}} \{L_q(X - t)\, e^{i\mu t} + L_q(X + t)\, e^{-i\mu t} - a_q - b_q t^2\} \\
& \times \exp\{-i\mu M(t^2 + Y^2)^{\frac{1}{2}}\} \left[\frac{1}{(t^2 + Y^2)^{\frac{3}{2}}} + \frac{i\mu M}{t^2 + Y^2}\right] dt \\
& + Y^2 \int_0^{\bar{t}} (a_q + b_q t^2)[\{1 + i\mu M(t^2 + Y^2)^{\frac{1}{2}}\} \\
& \times \exp\{-i\mu M(t^2 + Y^2)^{\frac{1}{2}}\} - 1 + \tfrac{1}{2}(i\mu M)^2(t^2 + Y^2)] \frac{dt}{(t^2 + Y^2)^{\frac{3}{2}}} \\
& + Y^2 \int_0^{\bar{t}} (a_q + b_q t^2)\{1 - \tfrac{1}{2}(i\mu M)^2(t^2 + Y^2)\} \frac{dt}{(t^2 + Y^2)^{\frac{3}{2}}} + Y^2 I,
\end{aligned}
\tag{I.21}
$$

where $\bar{t}$ is the smaller of X and $1 - X$,

$$
a_q = 2L_q(X), \qquad b_q = -\mu^2 L_q(X) - 2i\mu L_q'(X) + L_q''(X),
$$

and

$$
I = \int_X^{1-X} L_q(X + t) \exp\{-i\mu[t + M(t^2 + Y^2)^{\frac{1}{2}}]\} \left[\frac{1}{(t^2 + Y^2)^{\frac{3}{2}}} + \frac{i\mu M}{t^2 + Y^2}\right] dt
$$

or

$$
\int_{1-X}^{X} L_q(X - t) \exp\{i\mu[t - M(t^2 + Y^2)^{\frac{1}{2}}]\} \left[\frac{1}{(t^2 + Y^2)^{\frac{3}{2}}} + \frac{i\mu M}{t^2 + Y^2}\right] dt
$$

according as $X \leqslant \frac{1}{2}$ or $X > \frac{1}{2}$. In equation (I.21) all the integrands except the third are analytic at $t = 0$ and may be evaluated with $Y = 0$. The third integration may be carried out formally for general Y and expanded in the form of equation (28) to give

$$
\left.
\begin{aligned}
F_q(X, Y = 0) &= a_q \\
E_q(X) &= -b_q - \tfrac{1}{2} a_q \mu^2 M^2
\end{aligned}
\right\},
\tag{I.22}
$$

consistent with equations (30) and (55), and also the required term in Y^2. The contributions (I.13), (I.19), (I.20) and from T_3/Y^2 in (I.21) are added to give

$$
\begin{aligned}
D_q(X) = {} & L_q(1) \left[\tfrac{1}{2} \exp\{-i\mu(1 + M)(1 - X)\} \left(\frac{1}{(1 - X)^2} - \frac{i\mu(1 - M)}{1 - X}\right)\right. \\
& \left. + \tfrac{1}{2}\mu^2\beta^2 \left(\tfrac{1}{2}\pi i + \gamma + \ln\{\mu(1 + M)(1 - X)\} + \int_0^{\mu(1+M)(1-X)} v^{-1}(e^{-iv} - 1)\, dv\right)\right] \\
& + \int_0^{\bar{t}} \left[L_q(X + t) \exp\{-i\mu(1 + M)t\} + L_q(X - t) \exp\{i\mu(1 - M)t\} \left(\frac{1}{t^3} + \frac{i\mu M}{t^2}\right)\right. \\
& \left. - (a_q + b_q t^2)(1 + \tfrac{1}{2}\mu^2 M^2 t^2) t^{-3}\right] dt + a_q\{\tfrac{1}{2}\mu^2 M^2 \ln(2\bar{t}) - \tfrac{1}{2}(1/2\bar{t}^2)\} \\
& + b_q\{\ln(2\bar{t}) - 1 + \tfrac{1}{4}\mu^2 M^2 \bar{t}^2\} + I,
\end{aligned}
\tag{I.23}
$$

where

$$I = \int_X^{1-X} L_q(X + t) \exp\{-i\mu(1 + M)t\} \left[\frac{1}{t^3} + \frac{i\mu M}{t^2}\right] dt$$

or

$$\int_{1-X}^{X} L_q(X - t) \exp\{i\mu(1 - M)t\} \left[\frac{1}{t^3} + \frac{i\mu M}{t^2}\right] dt$$

according as $X \leqslant \frac{1}{2}$ or $X > \frac{1}{2}$.

The three integrations occurring in equation (I.23) will need to be performed numerically; in practice, a program was based on the method of Ref. 19. The first integrand, although analytic over the range, will be computed inaccurately near $v = 0$ due to cancellation, but the guarding figures inherent in a machine with a 39-bit word will more than compensate for such inaccuracies when only six or seven decimal places are required. In the second integrand, however, a severe cancellation will occur when the integrand is evaluated near $t = 0$, although again the integrand is analytic. The remedy here is to divide the range of integration $(0, \bar{t})$ into $(0, \kappa\bar{t})$ and $(\kappa\bar{t}, \bar{t})$, where, as suggested in Appendix II, $\kappa = 0{\cdot}5$ gives satisfactory results. The standard integration deals with the second range, but for the first it is necessary to resort to term-by-term integration of the Taylor series. The integrand of I is finite at the upper limit of integration, but has infinite derivatives at that point; provided a lower limit of 128 integration points is set ($\delta \geqslant 7$), sufficient accuracy is obtained.

APPENDIX II

Notes on Programs and Alternative Usage

By P. S. Hampton

The two programs have been written in KDF9 Usercode and, as such, are unique to an English Electric Leo–Marconi KDF9 machine.[21] The minimum use of peripheral equipment and the ability to calculate exact storage requirements allow greater efficiency of machine use in the time-sharing mode. All input and output routines are contained in English Electric library packages for KDF9 (e.g., Ref. 22), and the 8-hole input data tape must be compatible with the code used in these routines.

The respective flow diagrams for Programs I and II in Figs. 1 and 2 show alternative methods of operation depending on the planform and the required output. The four* types of planform, with or without artificial rounding of cranks, are defined by the parameters 'wing' and 'round' in Table II.1; the identifier 'sym' indicates whether the modes of deformation are symmetrical only, antisymmetrical only or of both kinds. The format of input data for Program I is listed in Table II.2, where provision is made for arbitrary numerical input modes in addition to the optional standard modes included in Table II.1. Checks are performed on the correctness of the data in amount and format, and the storage allocation is checked to prevent failure at a later stage. Failures lead to store prints, allowing the course of the program to be checked; the relevant failure messages are collected in Table II.3. Two parameters 'stop' and 'print' control the point at which Program I ends and the various output options (Table II.4a).

The main body of Program I employs influence function and integration subroutines written for KDF9 by Mr. A. R. Curtis. Entry parameters essential to the integration routine are as follows:

$\text{tol} = 10^{-\varepsilon}$, the tolerance of accuracy ($\varepsilon \geqslant 4$),

$n_{\max} = 2^{\delta}$, which limits the number of iterations if the tolerance has not been achieved ($\delta \geqslant 7$),

λ_{int}, the number of terms compared in the integration procedure with optimum value 3,

κ, a parameter for splitting the range of integration to deal with discontinuities; the suggested value is 0·5.

Having compiled the complex matrix $\Omega = \Omega_q(p, \nu, r)$, the program demands the solution $\Gamma = \Gamma_{qr}$ to the complex matrix equation $[\Omega][\Gamma] = [h]$ for right hand sides $h = h_{p\nu}$ corresponding to each input mode j. This has necessitated the writing of routines to deal with matrices in the complex field, and these routines have proved to be a valuable addition to the library of routines for use on KDF9.

Unless precluded by an instruction stop $\geqslant 1$ (Table II.4a), the final stage of Program I is the computation of complex generalized forces Q_{ij} corresponding to each input force mode Z_i. The numerical procedure of integration by quadrature varies in detail according as Z_i is a standard mode defined by formula (Table II.1), or a numerical mode defined by $Z_{p\nu}$ and the slopes $Z'_{p\nu}$ at all collocation positions. The facility print = 3 (Table II.4a) for outputting definitive wing data and the matrix from Program I on paper tape enables generalized forces for standard and numerical modes to be calculated quickly by means of Program II without the need to re-calculate the matrix. When additional or amended modes are envisaged, this should prove a valuable asset with computer time at a premium. With stop = 5 (Table II.4b), Program II goes on to calculate the load distribution and local lift and pitching moment at the sections $\eta = \eta_r$ and, if required, at arbitrary sections η_t; the format of input data is listed in Table II.5. The example in Appendix III illustrates the preparation of data tapes and the printed output in a computation involving both programs.

The storage requirement Σ for the two programs is restricted to the capacity of the KDF9 computer, so that $\Sigma \leqslant 29504$ or $\Sigma \leqslant 31456$ according as the programs are run in the time-sharing or non-time-

---

* A facility exists for a fifth type of planform (wing = 0), defined by a fifth degree spline fit and with provision for an elliptic tip.

sharing mode. The number of words of store needed for a particular computation depends upon the combination of the parameters (N, m, a) and the identifier sym. For Program I when sym = 1 or sym = −1, the storage $\Sigma = \Sigma_I$ is determined as

$$\Sigma_I = [8300 + 6n_{max} + (11N + 3N^2) + (4m^* + 3m^2) + 2Nm + (3\Lambda^* + 2N\Lambda + m\Lambda) + 2N^2R^2], \quad \text{(II.1)}$$

where $\Lambda = a(m + 1) - 1$, m^* and Λ^* are defined in Table II.2, and

$$\left.\begin{aligned} R &= \tfrac{1}{2}m && \text{for } m \text{ even and sym} = \pm 1 \\ &= \tfrac{1}{2}(m + 1) && \text{for } m \text{ odd and sym} = 1 \\ &= \tfrac{1}{2}(m - 1) && \text{for } m \text{ odd and sym} = -1 \end{aligned}\right\} \quad \text{(II.2)}$$

There is no difficulty with Program II, since smaller storage is required; whether sym = 1 or sym = −1 or −2 (Table II.5)

$$\Sigma = \Sigma_{II} = [\Sigma_I - 2000] \quad \text{(II.3)}$$

is sufficient. The facility in Program I of sym = 0, i.e., solutions sym = 1 followed by sym = −1, requires additional storage. The quantity Σ_I from equation (II.1) with sym = 1 is increased by an amount

$$\left.\begin{aligned} &N^2m\Lambda && \text{for } m \text{ even} \\ &N^2(m - 1)\Lambda && \text{for } m \text{ odd} \end{aligned}\right\}. \quad \text{(II.4)}$$

Thus, there is the penalty of an extra storage requirement of order N^2m^2a in Program I when sym = 0. A minor adjustment is made if $a = 1$ with m odd and sym = 1 or 0; in such cases the term given as $2N\Lambda$ in equation (II.1) is replaced by $2N(m + 1)$. The various combinations of the parameters (N, m, a) in Table II.6a illustrate some possible computations which lie within the time-sharing capacity $\Sigma_I \leqslant 29\,504$ for Program I with sym = 1 and $n_{max} = 128$ ($\delta = 7$). When sym = 0, the capacity restricts the use of Program I to much more limited combinations of (N, m, a) as is indicated by Table II.6b.

The basic storage requirement of each program, specified by the 8300 words in equation (II.1), includes 2000 words allocated for the input of Data 5 (Table II.2) for numerical modes Z_{num} and the retention of the complex coefficients Γ_{qr} for all modes j. Although some extra store of variable amount is also employed, there is a limit on the number of modes Z_{num} that can be accommodated for a specified combination (N, m, a); the greatest restrictions arise when sym = 0 and standard and numerical modes are input for both the symmetric and antisymmetric cases. It is noted that even with the failure message 'TOO MANY MODES' (Table II.3), the programs do not fail completely, but will proceed to evaluate Γ_{qr} for the maximum number of modes j consistent with the available store. It is not easy to define the limits on Z_{num} precisely; the following formulae are suggested as guide lines. Let

u = number of standard modes selected when sym = ± 1,

= number of symmetric standard modes when sym = 0, and

v = number of numerical modes when sym = 1, −1 or 0.

When sym = ± 1, the restriction on Input Data 5 gives

$$v \leqslant \frac{1000}{NR} \quad \text{(II.5)}$$

and there is an overall limitation on modes

$$u + 2v \leqslant \left[7 - N + m + a + \frac{1000}{NR}\right]. \tag{II.6}$$

When sym = 0, the limitation is

$$u + 2v \leqslant \left[2 + \frac{1000}{NR}\right] \quad \text{with } R \text{ for sym} = 1, \tag{II.7}$$

which is always more restrictive than the inequality of equation (II.5).

If the storage restrictions on Σ_1 are satisfied, the other consideration is the computer time to run Program I. This is mainly dependent on the size and accuracy of the matrix through the parameters (N, m, a) and (δ, ε), but it is found that the combination of Mach number M with aspect ratio A and frequency parameter $\bar{\nu}$ also influences the running time. From a correlation of times actually taken in seventy applications with $(\delta, \varepsilon) = (7, 4)$ and a limited number of applications with $(\delta, \varepsilon) = (8, 4), (7, 6), (8, 6)$, the empirical formula

$$\text{Running time} = (\tau N^{\frac{3}{2}} m^{\frac{3}{2}} a^{\frac{1}{2}}) \text{ seconds} \tag{II.8}$$

has been deduced to an accuracy of ± 10 per cent; for sym $= \pm 1$ the quantity τ approximates to

and

$$\left.\begin{aligned} \tau &= \frac{\sigma}{8}\left(\frac{\beta A + 2}{\beta A + 1}\right) && \text{for } \bar{\nu} = 0 \\ \tau &= \frac{\sigma}{4}\left(\frac{\beta A + 2}{\beta A + 1}\right)\left(0{\cdot}65 + 0{\cdot}04\frac{\bar{\nu}}{\beta^2}\right) && \text{for } \bar{\nu} > 0 \end{aligned}\right\} \tag{II.9}$$

with $\sigma = 4, 5, 7, 9$ for $(\delta, \varepsilon) = (7, 4), (8, 4), (7, 6), (8, 6)$ respectively.

An increase of up to 10 per cent in the value of σ should be allowed when sym = 0. With values $\tau = 1$ when sym = 1 and $\tau = 1{\cdot}2$ when sym = 0, appropriate to an example with

$$A = 6, \quad M = 0{\cdot}8\ (\beta = 0{\cdot}6), \quad \bar{\nu} = 1{\cdot}53 \quad \text{and} \quad (\delta, \varepsilon) = (7, 4),$$

the respective running times from equation (II.8) are given in Tables II.6a and II.6b for various examples just within the time-sharing mode. For large a, it is expected that the running time will become proportional to a; as equation (II.8) is likely to underestimate running times for $a > 8$, such estimates are omitted in Table II.6a. It seems, however, that capacity is a more severe restriction than running time, especially when sym = 0. Only in exceptional cases that might demand larger values of the accuracy parameters (δ, ε) would running time become the critical factor as a result of the increase in σ. For the examples given in this Report $(\delta, \varepsilon) = (7, 4)$ gives sufficient accuracy for the specified combinations (N, m, a). To ensure completion of a long run, it is suggested that 10 per cent should be added to the estimated time in the operating instructions.

APPENDIX III

Illustrative Example

The example for the elliptical wing at $M = 0{\cdot}8$ with $N, m, a = 3, 5, 2$, used for the desk calculations discussed in Section 5.1, is convenient in size and scope to illustrate the input and output as summarized in Tables II.1 and II.5. Since the planform has continuous non-zero curvature, we set wing = 4 and round = 0. The calculation will include symmetric and antisymmetric standard modes, so that sym = 0. From Table II.4a, we choose stop = 0 and print = 3, so that the generalized forces are calculated in Program I and the output tape provides the aerodynamic influence matrices (symmetric and antisymmetric) for Program II.

With reference to Table II.2 and the planform data in Table 1, Data 1 and 2 are input and then output as shown at the top of Table III.1. As reference length, the semi-span s is unity; the frequency parameter $k = \omega s/U = 1$ becomes $\bar{\nu} = \omega\bar{c}/U = 0{\cdot}3\pi$. Instead of at the centre of the ellipse as in Fig. 3, the origin is taken at the leading edge of the centre section, and Data 3 require prior evaluation of

$$\left.\begin{aligned} x_{l\lambda} &= 0{\cdot}6\left[1 - \sin\left(\frac{\lambda\pi}{\Lambda+1}\right)\right] \\ c_\lambda &= 1{\cdot}2\sin\left(\frac{\lambda\pi}{\Lambda+1}\right) \end{aligned}\right\} \lambda = 1(1)\Lambda^*,$$

where $\Lambda + 1 = a(m+1) = 12$ and $\Lambda^* = 6$, and

$$\left.\begin{aligned} x'_{lv} &= -0{\cdot}6\cot\left(\frac{v\pi}{m+1}\right), & x''_{lv} &= 0{\cdot}6\,\mathrm{cosec}^3\left(\frac{v\pi}{m+1}\right) \\ c'_v &= 1{\cdot}2\cot\left(\frac{v\pi}{m+1}\right), & c''_v &= -1{\cdot}2\,\mathrm{cosec}^3\left(\frac{v\pi}{m+1}\right) \end{aligned}\right\} v = 1(1)3.$$

These also appear in Table III.1, followed by the definition of the symmetric and antisymmetric modes i or j corresponding to Data 4

$$\left.\begin{aligned} &1;1;0;0;0;1;0;0;0;0;0;0;0;0;0; \\ &1;1;0;0;0;0;0;0;0;0;0; \end{aligned}\right\}.$$

Data 5 (including ζ) are omitted as there are no numerical input modes. The storage is then calculated, so that failure from insufficient storage would preclude the start of the main computation (Table II.3).

The remainder of the output from Program I, described in Table II.4a, consists of the symmetric matrix $[\Omega]$ with elements $\Omega_q(p, v, r)$ (Table III.2), the solutions $[\Gamma]$ with elements $(\Gamma_{qr})_j$ and the matrix of generalised force coefficients Q_{ij} (Table III.3), followed by the corresponding antisymmetric results (not illustrated). Each row in Table III.2 represents the real and imaginary parts of $\Omega_q(p, v, r)$ first with $v = 1$ and then with $v = 2$ and 3, while the last three rows in Table III.3 give similarly the real and imaginary parts of Q_{ij}, viz., $Q'_{i1}, kQ''_{i1}, Q'_{i2}, kQ''_{i2}, Q'_{i3}, kQ''_{i3}$.

The input for Program II is listed in Table II.5. The first half of the output tape from Program I is detached to provide input tape A for the symmetrical case sym = 1. Input tape B requires Data 8 and 9; thus stop = 5, $V = 8$ and $T = 3$ indicate that load distributions are to be obtained at local chordwise positions

$$\xi = \frac{1}{2}\left(1 + \cos\frac{v\pi}{V}\right), \qquad v = 1, 2, \ldots (V-1)$$

at 3 sections in addition to the loading sections $\eta = \eta_r$. Then Data 10 of Table II.5 specify η_t, x_{lt} and c_t at these 3 sections, so that the loading can be evaluated from equations (51), (53) and (86). To reduce output, only the first two standard modes are included in Data 4 and again Data 5 are omitted in the absence of numerical modes.

Table II.4b summarizes the complete output from Program II, the initial and final parts of which are reproduced in Table III.4. For each value of ξ the real and imaginary parts of $(l_r)_j$ are given side by side for the appropriate values of η_r and η_t. The corresponding local lifts and moments are computed from equations (87) and (89) with interpolation from equation (53) as necessary. Separate tables are printed for each value of j. The short running time of 15 seconds illustrates that this is trivial by comparison with that of Program I.

TABLE 1

Planforms used in Numerical Examples

Planform	Elliptic	Tapered swept	Rectangular	Tapered swept
A	$20/(3\pi)$	2	1·250	6
s	1	1	0·625	3
$\bar{c}$	$0{\cdot}3\pi$	1	1	1
x_{lR}	−0·6	−0·808013	0	0
c_R	1·2	1·616025	1	1·5
x_{lT}	0	0·924038	0	2·232051
c_T	0	0·383975	1	0·5
round	0	1	1	1
η_{iR}	—	0·195090	any	0·195090
d	s	s	$\bar{c}$	$\bar{c}$
D	s^2	s^2	$2s\bar{c}$	$2s\bar{c}$

TABLE 2

Generalised Forces for Elliptic Wing ($M = 0{\cdot}8$, $k = \omega s/U = 1$)

Solutions with $(N, m, a) = (4, 11, 6)$, $(\delta, \varepsilon) = (8, 6)$ and origin at centre of ellipse

(a) *Symmetric modes*

i	$Z = 1$		$Z = X$		$Z = X^2$		$Z = Y^2$	
	Q'_{i1}	Q''_{i1}	Q'_{i2}	Q''_{i2}	Q'_{i3}	Q''_{i3}	Q'_{i4}	Q''_{i4}
1	−0·8731	3·2056	3·7071	1·6371	1·5810	−0·6271	−0·1308	0·7563
2	−0·5013	−0·7636	−0·8969	0·9203	0·8256	0·3167	−0·1111	−0·1412
3	0·0531	0·3759	0·3883	−0·1033	−0·1035	0·0384	0·0180	0·0660
4	−0·1308	0·7563	0·8675	0·2722	0·3008	−0·1563	−0·0532	0·2450

(b) *Antisymmetric modes*

i	$Z = Y$		$Z = XY$	
	Q'_{i1}	Q''_{i1}	Q'_{i2}	Q''_{i2}
1	−0·2123	0·4084	0·4261	0·3291
2	−0·0177	−0·1166	−0·1309	0·0553

TABLE 3

Generalised Forces for Tapered Swept Wing ($A = 2$, $M = 0{\cdot}7806$, $\bar{\nu} = 1$)

Origin at mid-root-chord

(a) *Present solutions*

Force mode	N	m	a	δ	ε	$Z = 1$		$Z = X$	
						Q'_{i1}	Q''_{i1}	Q'_{i2}	Q''_{i2}
$Z = 1$ $i = 1$	3	15	2	7	4	−0·7289	2·5815	2·6549	2·7488
	3	15	3	8	6	−0·7291	2·5821	2·6551	2·7492
	3	14	3	8	6	−0·7312	2·5802	2·6507	2·7532
	3	14	3	7	4	−0·7311	2·5802	2·6506	2·7532
	4	14	3	7	4	−0·7268	2·5990	2·6944	2·7632
$Z = X$ $i = 2$	3	15	2	7	4	−0·4952	0·7390	0·5218	1·6661
	3	15	3	8	6	−0·4956	0·7389	0·5215	1·6660
	3	14	3	8	6	−0·4933	0·7374	0·5194	1·6609
	3	14	3	7	4	−0·4933	0·7374	0·5194	1·6609
	4	14	3	7	4	−0·5086	0·7548	0·5399	1·7111

(b) *Comparisons with other methods*

Method	Q'_{11}	Q''_{11}	Q'_{12}	Q''_{12}	Q'_{21}	Q''_{21}	Q'_{22}	Q''_{22}
$N = 3$								
Ref. 3	−0·742	2·588	2·640	2·765	−0·496	0·735	0·511	1·650
Ref. 15	−0·726	2·600	2·679	2·748	−0·512	0·741	0·515	1·686
Present	−0·729	2·582	2·655	2·749	−0·496	0·739	0·522	1·666
$N = 4$								
Ref. 13	−0·687	2·554	2·635	2·744	−0·494	0·710	0·480	1·668
Ref. 7	−0·747	2·616	2·706	2·802	−0·506	0·740	0·517	1·704
Present	−0·727	2·599	2·694	2·763	−0·509	0·755	0·540	1·711

TABLE 4

Heaving and Pitching Derivatives for Rectangular Wing ($A = 1{\cdot}25$, $M = 0$)

Solutions with $m = 11$ and pitching axis $x_0 = 0$

$\bar{\nu}$	N	a	δ	ε	Q'_{11}	Q''_{11}	Q'_{12}	Q''_{12}	Q'_{21}	Q''_{21}	Q'_{22}	Q''_{22}
1·5	3	4	7	4	−1·0768	0·8365	0·3147	1·1620	−0·5548	0·1536	−0·1670	0·5301
	3	6	7	4	−1·0763	0·8364	0·3150	1·1617	−0·5545	0·1537	−0·1667	0·5301
	4	6	7	4	−1·0783	0·8369	0·3154	1·1632	−0·5567	0·1530	−0·1691	0·5326
	5	6	7	4	−1·0786	0·8371	0·3154	1·1635	−0·5569	0·1530	−0·1693	0·5327
	5	6	8	4	−1·0786	0·8371	0·3153	1·1635	−0·5569	0·1530	−0·1693	0·5327
	5	6	8	6	−1·0786	0·8371	0·3153	1·1635	−0·5568	0·1530	−0·1693	0·5327
6·0	3	6	7	4	−11·2885	0·0853	−6·1793	0·3426	−4·6912	0·1180	−2·7647	0·2218
	4	4	7	4	−16·3973	0·5492	−8·0731	0·8870	−7·6697	0·1333	−4·4216	0·4054
	5	4	7	4	−17·8113	0·7592	−8·2209	1·1120	−8·8104	0·1441	−5·0071	0·5044
	6	4	7	4	−17·9991	0·7978	−8·1735	1·1516	−9·0217	0·1464	−5·1090	0·5280
	7	4	7	4	−18·0093	0·8013	−8·1621	1·1550	−9·0413	0·1465	−5·1184	0·5307
6·0	4	4	7	4	−16·3973	0·5492	−8·0731	0·8870	−7·6697	0·1333	−4·4216	0·4054
	4	4	8	4	−16·3972	0·5492	−8·0731	0·8870	−7·6697	0·1333	−4·4216	0·4054
	4	4	8	6	−16·3972	0·5492	−8·0730	0·8870	−7·6697	0·1333	−4·4216	0·4054
	4	6	8	6	−16·4007	0·5492	−8·0752	0·8872	−7·6718	0·1333	−4·4230	0·4055

TABLE 5

Heaving and Pitching Derivatives for Tapered Swept Wing ($A = 6$, $M = 0{\cdot}4$)

Solutions with $N = 6$, $(\delta, \varepsilon) = (7, 4)$ and axis at root leading edge

(a) $(N, m, a) = (6, 15, 4)$

$\bar{\nu}$	Q'_{11}	Q''_{11}	Q'_{12}	Q''_{12}	Q'_{21}	Q''_{21}	Q'_{22}	Q''_{22}
0·0001	0·0000	2·0979	2·0979	2·7948	0·0000	2·6398	2·6398	4·0197
0·2484	0·0225	1·9611	2·0150	3·0550	0·0262	2·4581	2·5163	4·3541
0·5000	−0·0010	1·7972	1·8613	3·1466	−0·0162	2·2378	2·2682	4·4714
1·0257	−0·3903	1·6330	1·2626	3·2231	−0·5854	2·0098	1·2758	4·5647
1·6085	−1·3572	1·6409	0·0861	3·3509	−1·9816	2·0036	−0·6919	4·7281
2·2936	−3·1373	1·8168	−1·9268	3·6223	−4·5850	2·2107	−4·1413	5·0941
3·1569	−6·0487	2·2581	−5·0469	4·1338	−9·0342	2·7699	−9·8289	5·8320
4·3451	−9·8930	3·0458	−9·3838	4·9274	−15·6069	3·8874	−18·6114	7·1461

(b) $\bar{\nu} = 3{\cdot}1569$

Method	m	a	Q'_{11}	Q''_{11}	Q'_{12}	Q''_{12}	Q'_{21}	Q''_{21}	Q'_{22}	Q''_{22}
Direct	14	6	−6·2908	2·2318	−5·3548	4·1850	−9·2140	2·7331	−10·1222	5·8539
	15	6	−6·0688	2·2643	−5·0652	4·1452	−9·0664	2·7773	−9·8672	5·8479
	22	4	−6·2283	2·2683	−5·1966	4·1949	−9·2024	2·7683	−10·0157	5·8784
	23	4	−6·1401	2·2743	−5·0909	4·1806	−9·1228	2·7791	−9·9064	5·8716
Reverse flow	15	6	−6·2951	2·2470	−5·3040	4·1991	−9·2182	2·7455	−10·0917	5·8695
	23	4	−6·2226	2·2667	−5·1945	4·1938	−9·1977	2·7682	−10·0159	5·8804

TABLE 6

Heaving and Pitching Derivatives for Tapered Swept Wing ($A = 6$, $M = 0{\cdot}8$)

Solutions with $m = 15$, $(\delta, \varepsilon) = (7, 4)$ and axis at root leading edge

N	a	$\bar{v}$	Q'_{11}	Q''_{11}	Q'_{12}	Q''_{12}	Q'_{21}	Q''_{21}	Q'_{22}	Q''_{22}
6	4	0·0001	0·0000	2·5505	2·5505	2·1404	0·0000	3·2483	3·2483	3·5731
		0·2484	0·0812	2·2790	2·4532	2·6382	0·0888	2·9087	3·1018	4·2255
		0·5000	0·1422	2·0071	2·3723	2·8476	0·1242	2·5770	2·9378	4·5315
		1·0257	0·0205	1·8595	2·2495	2·9701	−0·2088	2·4549	2·5960	4·8105
		1·6085	−0·2648	1·8948	2·0313	3·0067	−0·7836	2·6211	2·1521	4·9511
		2·2936	−0·6104	1·9864	1·7379	3·0579	−1·3808	2·8390	1·5956	5·0871
		3·1569	−1·1343	2·0790	1·1315	3·1148	−2·2012	3·0113	0·5531	5·1981
		4·3451	−1·8024	2·2413	0·1334	3·2659	−3·2530	3·2943	−1·1774	5·4744
4	4	4·3451	−1·8407	2·4433	0·7881	3·6158	−3·4001	3·4617	−0·8504	5·8266
5	4		−1·5743	2·2245	0·5549	3·2144	−3·0410	3·2923	−0·7541	5·4551
6	4		−1·8024	2·2413	0·1334	3·2659	−3·2530	3·2943	−1·1774	5·4744
7	4		−1·7425	2·2489	0·2266	3·2815	−3·2309	3·3054	−1·1457	5·4968
7	6		−1·7471	2·2552	0·2289	3·2917	−3·2397	3·3154	−1·1476	5·5140

TABLE 7

Direct Comparison of Computations by Present Method and that of Ref. 7

Tapered swept wing $A = 6$, $M = 0{\cdot}4$, $\bar{v} = 3{\cdot}1569$, $N = 6$, $m = 14$

Method	Ref. 7			Present	
	$q = 1$	$q = 5$	$q = 9$	$a = 6$	$a = 10$
Q'_{11}	−5·661	−6·398	−6·354	−6·291	−6·297
Q''_{11}	2·098	2·259	2·250	2·232	2·234
Q'_{12}	−4·646	−5·376	−5·354	−5·355	−5·364
Q''_{12}	3·849	4·226	4·216	4·185	4·190
Q'_{21}	−8·273	−9·322	−9·276	−9·214	−9·228
Q''_{21}	2·542	2·740	2·741	2·733	2·736
Q'_{22}	−8·890	−10·203	−10·167	−10·122	−10·143
Q''_{22}	5·367	5·877	5·878	5·854	5·862
Time in minutes	5	64	113	29	44

TABLE II.1

Definitions of Wing, Round and Standard Modes

wing = 1	Planform of arbitrary aspect ratio, taper ratio and sweepback (crank at $\eta = 0$)
wing = 2	As wing = 1 with additional crank at $\lvert\eta\rvert = \eta_K$
wing = 3	As wing = 1 with additional cranks at $\lvert\eta\rvert = \eta_A$ and $\lvert\eta\rvert = \eta_B$
wing = 4	Planform with arbitrary curvature, defined by numerical input $x_{l\lambda}$, c_λ, x'_{lv}, x''_{lv}, c'_v, c''_v
round = 0	Case where wing = 4 and round $\neq 1$, $\neq 2$
round = 1	Artificial rounding from equation (68) at all cranks
round = 2	Artificial rounding from equation (69) at all cranks

	Optional standard modes $Z(X = x/d, Y = y/s)$
sym = 1	$1, X, X^2, X^3, X^4, Y^2, XY^2, X^2Y^2, X^3Y^2, Y^4, XY^4, X^2Y^4, Y^6, XY^6, Y^8$
sym = −1	$Y, XY, X^2Y, X^3Y, Y^3, XY^3, X^2Y^3, Y^5, XY^5, Y^7$
sym = 0	15 modes for sym = 1 and 10 modes for sym = −1

TABLE II.2

Format of Input Data Tape for Program I

Data	Case	Input tape, with Data 5 if any	Fig. 1a
1		Descriptive title with end message	
2		M; $\bar{\nu}$; sym; N; m; a; $n_{\max}$; tol; λ_{int}; κ;	Initial data
		stop; print; wing; round; s; $\bar{c}$; D;	Stop and print values in Table B4
3	wing = 1	x_{lR}; c_R; η_{iR}; x_{lT}; c_T;	Additional data appropriate to value of wing. Wing and round are defined in Table (II.1)
	wing = 2	x_{lR}; c_R; η_{iR}; η_K; x_{lK}; c_K; η_{iK}; x_{lT}; c_T;	
	wing = 3	x_{lR}; c_R; η_{iR}; η_A; x_{lA}; c_A; η_{iA}; η_B; x_{lB}; c_B; η_{iB}; x_{lT}; c_T;	
	wing = 4†	$x_{l\lambda}$; ..... c_λ; ..... x'_{lv}; ..... x''_{lv}; ..... c'_v; ..... c''_v;	
4	sym = 1	1 (or 0); ..... 15 times.....	Indicators 1 (Yes) or 0 (No) used for standard modes in Table (II.1)
	sym = −1	1 (or 0); ..... 10 times.....	
	sym = 0	1 (or 0); ..... 25 times.....	
5	sym = 0	ζ; (= number of symmetric modes Z_{num})	Omit if sym = ± 1
		Z'_{pv}; Z_{pv}; ..... (pv = 11, 12, ... 1R, 21, 22, ... NR)	Numerical input modes, all Z_{num}. R from eqn. II.2
		End message	

† $\lambda = 1(1)\Lambda^*$ where $\Lambda^* = \frac{1}{2}\Lambda$ or $\frac{1}{2}(\Lambda + 1)$ according as Λ is even or odd, and $v = 1(1)m^*$ where $m^* = \frac{1}{2}m$ or $\frac{1}{2}(m + 1)$ according as m is even or odd.

TABLE II.3

Messages on Printout for Failure of Programs I and II

Message output	Reason for failure	Remarks
NEGATIVE NUMBER— IN DATA	Negative number in initial data excluding sym, on input tape	Applies only to Program I
BASIC PM ..... with 271 in top row of nesting store	Insufficient standard mode data	Insufficient data or incorrect format of input tape with no Data 5
R.H.S. FAIL	Wrong amount of numerical mode data	Can arise from excess standard mode data
STORAGE EXC.	Allocated storage insufficient	Required STORAGE ..... printed on previous line
SERIES OVERFLOW BASIC PM	Store exceeded in a calculation of $F_q(p, v, \lambda)$	Applies only to Program I. Matrix store printed out
MATRIX FAIL	Singular matrix generated	Matrix expected to be well conditioned
TOO MANY MODES	Store insufficient for Data 5 and all $(\Gamma_{qr})_j$. See equations (II.5) to (II.7)	Message replaces $(\Gamma_{qr})_j$ where excess modes j are ignored. Calculation continues to end

TABLE II.4

Output for Alternative Combinations of Stop and Print

(a) *Program I*

	* Additional output	Extent of calculation			
		Q_{ij}	$(\Gamma_{qr})_j$	$\Omega_q(p, v, r)$	Data 6
		stop = 0	stop = 1	stop = 2	stop = 3
print = 0	—	√	√		√
print = 1	$\Omega_q(p, v, r)$ h_{pv} if stop $\leqslant 1$	√	√	√	
print = 2	$\Omega_q(p, v, r)$ h_{pv} if stop $\leqslant 1$ $(K_{qr})_i$	√			
print = 3	$\Omega_q(p, v, r)$ Output tape	√	√	√	
print = 4	$F_q(p, v, \lambda)$ $D_q(p, v)$ $\Omega_q(p, v, r)$	√	√	√	

* Compulsory output is defined by stop and the following data:
Data (1 + 2) of Table II.2 plus Data (3 + 6) of Table II.5 with sym = 1 or −1 or 0;
Modes i, j (= 1, 2, 3 . . .) given by Data 4 (indicator 1) and Data 5 (if any) of Table II.2;
storage Σ; $(\Gamma_{qr})_j$; Q_{ij}; running time in seconds.

(b) *Program II*

	Extent of calculation and output
stop = 0	Q_{ij} [sym = 1 or sym = − 1(−2)] Output for print = 2 of Program I
stop = 5	As above but also loading at η_r, and at η_t (optional)

TABLE II.5

Format of Input Data Tape (A + B) for Program II

The output from Program I with print = 3 gives tape A labelled as follows:

Program I	Input tape A with matrix	
	Symmetric	Antisymmetric
sym = 1	sym = 1	—
sym = −1	—	sym = −1
sym = 0	sym = 1	sym = −2

Data	Input tape A	Remarks
1	Descriptive title with end message	To be inserted by hand if sym = −2
2	Data 2 of Table II.2	Excluding stop and print
3	Data 3 of Table II.2	Only if wing ≠ 4
6	Data 3 of Table II.2 for wing = 4 preceded by η_λ;	wing = 1, 2, 3 or 4
7	Real; imaginary; ..... elements of matrix $\Omega_q(p, v, r)$	
	Delete end message, if any	Cut tape before Data 2 with sym = −2

Data	Input tape B	Remarks
8	stop (= 0 or 5);	See Table II.4b
9	V; T ($\geqslant 0$);	Only if stop = 5
10	η_t; x_{lt}; c_t;	Only if $T \geqslant 1$ Repeat for t = 1(1)T
4	Data 4 of Table II.2	Treat sym = −2 as sym = −1
5	Data 5 of Table II.2	
	End message	

TABLE II.6

Usable (N, m, a) and Running Times with $\delta = 7$ in Time-Sharing Mode

(a) $sym = 1$

N	m	a	Eqn. (II.8) with $\tau = 1$
$\leqslant 5$	31	3	$\leqslant 56$ min
$\leqslant 7$	23	4	$\leqslant 68$ min
$\leqslant 10$	15	6	$\leqslant 75$ min
4	$\leqslant 38$	2	$\leqslant 44$ min
4	$\leqslant 34$	4	$\leqslant 53$ min
4	$\leqslant 30$	8	$\leqslant 62$ min
4	23	$\leqslant 17$	
4	15	$\leqslant 44$	
4	11	$\leqslant 76$	

(b) $sym = 0$

N	m	a	Eqn. (II.8) with $\tau = 1{\cdot}2$
$\leqslant 2$	23	4	$\leqslant 12$ min
4	$\leqslant 15$	4	$\leqslant 19$ min
4	11	$\leqslant 8$	$\leqslant 17$ min

TABLE III.1

ILLUSTRATIVE EXAMPLE - ELLIPTIC WING

MACH= 8.00000E- 1
FREQ= 9.42478E- 1
SYM= 0
N= 3.00000
M= 5.00000
A= 2.00000
NMAX= 25
TOL= 1.00000E- 6
LINT= 3.00000
K= 5.00000E- 1
STOP= 0
PRINT= 3

WING= 4
ROUND= 0
S= 1.00000
CBAR= 9.42478E- 1
AREA= 1.00000

COLLOCATION PTS

ETA	XL	C	XLDASH	CDASH	XL DOUBLE DASH	C DOUBLE DASH
-9.65926E- 1	4.44709E- 1	3.10583E- 1				
-8.66025E- 1	3.00000E- 1	6.00000E- 1	-1.03923	2.07846	4.80000	-9.60000
-7.07107E- 1	1.75736E- 1	8.48528E- 1				
-5.00000E- 1	8.03848E- 2	1.03923	-3.46410E- 1	6.92820E- 1	9.23760E- 1	-1.84752
-2.58819E- 1	2.04445E- 2	1.15911				
4.91696E-12	0.00000	1.20000	0.00000	0.00000	6.00000E- 1	-1.20000

MODES SYMMETRY

IJ=1 Z=1

IJ=2 Z=X

IJ=3 $Z=Y^2$

ANTI-SYMMETRY

IJ=1 Z=Y

IJ=2 Z=XY

STORAGE 10678 WORDS

SYMMETRIC MATRIX OMEGA

Q	R	P= 1					
1	1	4.77785	4.70685E- 1	-3.76940E- 1	1.33523E- 1	1.27138E- 1	5.02067E- 2
	2	-2.04045	2.18970E- 1	2.41164	5.14263E- 1	-9.18313E- 1	2.89926E- 1
	3	3.74830E- 1	7.08714E- 2	-7.11650E- 1	1.53974E- 1	1.97063	4.51112E- 1
2	1	3.76629	1.48489E- 1	-3.19211E- 1	6.36151E- 2	7.14394E- 2	2.62706E- 2
	2	-1.17246	3.24018E- 2	1.87390	2.01174E- 1	-7.12012E- 1	1.36372E- 1
	3	1.71658E- 1	2.59085E- 2	-4.87901E- 1	5.21877E- 2	1.55368	1.71815E- 1
3	1	1.84790	-1.25166E- 1	-1.88920E- 1	4.94741E- 3	3.22416E- 2	4.09975E- 3
	2	-4.28971E- 2	-8.96959E- 2	9.64009E- 1	-1.28156E- 1	-3.46430E- 1	-2.16400E- 2
	3	-5.77590E- 2	-4.77861E- 3	-1.52232E- 1	-3.97406E- 2	8.26706E- 1	-1.33004E- 1
		P= 2					
1	1	5.48199	2.66010E- 1	-1.07022	1.20788E- 1	8.56676E- 2	8.47857E- 2
	2	-1.73120	1.67193E- 1	3.34206	2.77543E- 1	-1.83669	2.02996E- 1
	3	4.30314E- 2	6.94183E- 2	-1.04241	1.09216E- 1	2.89239	2.16979E- 1
2	1	1.71013	-1.87310E- 1	-2.64350E- 1	-3.40781E- 2	1.61909E- 2	-3.21486E- 3
	2	-7.30704E- 1	-4.83295E- 2	9.06990E- 1	-1.88382E- 1	-5.31735E- 1	-8.20269E- 2
	3	5.65647E- 2	-1.51684E- 3	-3.37524E- 1	-4.36157E- 2	7.77368E- 1	-1.84759E- 1

—continued

TABLE III.2—*continued*

3	1	-1.30461	-5.56900E- 2	1.35084E- 1	-1.10711E- 2	-2.69966E- 2	-5.20430E- 3
	2	2.46355E- 1	-5.54099E- 2	-7.42094E- 1	-7.45476E- 2	2.55892E- 1	-4.48745E- 2
	3	-2.46795E- 2	-1.46313E- 2	1.47114E- 1	-3.31546E- 2	-6.27320E- 1	-6.76992E- 2
		P= 3					
1	1	6.28743	1.24986E- 1	-1.24243	6.08489E- 2	5.89432E- 2	5.06683E- 2
	2	-1.96728	1.35596E- 1	3.75079	1.28945E- 1	-2.11345	9.82002E- 2
	3	4.18602E- 2	5.60494E- 2	-1.19435	6.46112E- 2	3.25284	8.57079E- 2
2	1	-2.19628E- 1	-1.13816E- 1	-1.34827E- 2	-2.23155E- 2	-6.03722E- 3	-1.23129E- 2
	2	-4.63331E- 1	-8.37344E- 2	-9.17928E- 2	-1.33459E- 1	-7.50588E- 2	-7.73264E- 2
	3	6.05748E- 2	-1.17679E- 2	-1.04434E- 1	-5.56740E- 2	-6.97832E- 2	-1.21115E- 1
3	1	3.71374E- 2	8.46948E- 2	2.47913E- 3	6.46428E- 3	-2.55202E- 3	-7.79376E- 4
	2	4.78126E- 1	1.04589E- 2	2.46896E- 2	9.05928E- 2	7.18703E- 2	2.76737E- 2
	3	-1.19327E- 1	-1.41454E- 2	1.09286E- 1	1.76389E- 2	3.47166E- 2	9.58150E- 2

TABLE III.3

GAMMA

	PEAL	IMAGINARY
J= 1		
	-1.95777 37087E- 1	3.58815 11761E- 1
	-4.37168 33527E- 1	5.51980 52758E- 1
	-5.44302 61490E- 1	5.97618 58320E- 1
	2.48677 81907E- 1	2.07760 46969E- 1
	7.53061 93109E- 1	5.09824 66197E- 1
	1.00289 38384	6.75434 55287E- 1
	4.03930 27961E- 2	-4.30148 78868E- 2
	1.63984 69034E- 1	-3.10623 25796E- 1
	2.42224 12786E- 1	-5.03209 06710E- 1
J= 2		
	2.40822 78630E- 1	4.76306 43416E- 1
	2.05447 70466E- 1	9.36207 39764E- 1
	1.31416 06866E- 1	1.11514 01121
	4.70536 88781E- 1	-2.97612 98291E- 1
	1.34585 69935	-9.01503 12306E- 1
	1.81485 44477	-1.17538 64517
	-7.23325 04844E- 2	-1.06025 24875E- 1
	-5.06457 55829E- 1	-5.41529 81959E- 1
	-7.95256 70286E- 1	-8.32383 71539E- 1
J= 3		
	-1.07695 92826E- 1	1.42104 44778E- 1
	-1.00930 71498E- 1	1.35171 63446E- 1
	-5.49903 86077E- 2	1.07624 73367E- 1
	8.02913 89280E- 2	1.11659 32160E- 1
	1.74466 81647E- 1	9.63127 13495E- 2
	1.78625 71946E- 1	1.81554 59619E- 2
	1.93443 25870E- 2	-9.36081 65766E- 3
	3.66493 34341E- 2	-8.33045 22858E- 2
	1.66338 99023E- 2	-1.16610 44549E- 1

SYMMETRIC

Q					
IJ					
-8.83128E- 1	3.19632	3.15390	3.57177	-1.37527E- 1	7.55369E- 1
Q					
IJ					
-1.01441	1.14722	6.94607E- 1	2.56663	-1.89461E- 1	3.08913E- 1
Q					
IJ					
-1.36121E- 1	7.55631E- 1	7.81503E- 1	7.34424E- 1	-5.68915E- 2	2.45348E- 1

E= 203

TABLE III.4

STOP= 5

V= 8
Y= 3

ETA	X	C
T	LT	T
3.00000E- 1	2.76365E- 2	1.14473
7.00000E- 1	1.71514E- 1	8.56971E- 1
9.00000E- 1	3.38466E- 1	5.23068E- 1

J= 1 LOAD DISTRIBUTION

XI	ETA= -8.660254E- 1		ETA= -5.000000E- 1		ETA= 0.000000	
9.619398E- 1	-6.65124E- 1	2.50420E- 1	-1.40310	2.90762E- 1	-1.74405	3.21477E- 1
8.535534E- 1	-1.15956	5.93093E- 1	-2.28104	7.19969E- 1	-2.77564	7.60889E- 1
6.913417E- 1	-1.37200	1.10418	-2.49137	1.47974	-2.94150	1.59363
5.000000E- 1	-1.23327	1.84169	-2.23955	2.60328	-2.62431	2.88914
3.086583E- 1	-6.26727E- 1	2.92122	-1.56817	3.88457	-1.76674	4.28210
1.464466E- 1	7.54406E- 1	4.81302	1.08564E+ 1	5.41613	-1.83684E- 1	5.68247
3.806023E- 2	4.22357	1.00746E+ 1	4.78198	9.39595	5.15357	9.21772
LIFT	-1.90391E- 1	3.01208	-9.65040E- 1	3.40192	-1.26833	3.56530
MOMENT	4.86306E- 1	-6.97909E- 1	9.75972E- 1	-9.01989E- 1	1.18065	-9.78570E- 1

XI	ETA= 3.000000E- 1		ETA= 7.000000E- 1		ETA= 9.000000E- 1	
9.619398E- 1	-1.62344	3.10734E- 1	-1.05767	2.63661E- 1	-5.73098E- 1	2.51794E- 1
8.535534E- 1	-2.60241	7.49340E- 1	-1.76495	6.61174E- 1	-1.01419	5.79223E- 1
6.913417E- 1	-2.78753	1.55923	-1.99136	1.32069	-1.21799	1.04914
5.000000E- 1	-2.49489	2.79352	-1.79593	2.26931	-1.09130	1.73329
3.086583E- 1	-1.82880	4.14472	-1.14094	3.45285	-4.98557E- 1	2.78765
1.464466E- 1	-7.83740E- 2	5.58870	3.96432E- 1	5.14151	8.56271E- 1	4.72878
3.806023E- 2	5.02552	9.27092	4.42519	9.66801	4.25602	1.01739E+ 1
LIFT	-1.16355	3.50936	-6.30348E- 1	3.22440	-6.93059E- 2	2.95879
MOMENT	1.10989	-9.53278E- 1	7.54830E- 1	-8.11350E- 1	4.19834E- 1	-6.69912E- 1

—continued

TABLE III.4—*continued*

J= 2 LOAD DISTRIBUTION

XI	ETA= -8.660254E- 1		ETA= -5.000000E- 1		ETA= 0.000000	
9.619398E- 1	-1.93615E- 1	1.38424	-8.15069E- 1	2.76181	-1.08570	3.40893
8.535534E- 1	-9.59670E- 2	2.50033	-9.48361E- 1	4.60536	-1.35939	5.52104
6.913417E- 1	4.75101E- 1	3.20922	6.04649E- 2	5.42462	-1.77693E- 1	6.27993
5.000000E- 1	1.55743	3.45945	2.00977	5.68880	2.18632	6.53375
3.086583E- 1	3.20052	3.13217	4.20262	5.33391	4.63335	6.28475
1.464466E- 1	5.95538	1.96043	6.67245	3.20461	6.98797	3.82226
3.806023E- 2	1.32252E+ 1	-7.35774E- 1	1.27596E+ 1	-3.21035	1.28246E+ 1	-4.35400
LIFT	3.29191	2.39815	3.34169	3.83584	3.38068	4.41646
MOMENT	-5.25230E- 1	-1.35160	-4.41061E- 1	-2.33883	-3.90975E- 1	-2.74687

XI	ETA= 3.000000E- 1		ETA= 7.000000E- 1		ETA= 9.000000E- 1	
9.619398E- 1	-9.89246E- 1	3.18006	-5.37553E- 1	2.10997	-1.05044E- 1	1.21784
8.535534E- 1	-1.20972	5.20271	-5.54272E- 1	3.63623	1.80682E- 2	2.22963
6.913417E- 1	-8.76844E- 2	5.99161	2.63181E- 1	4.44385	5.25117E- 1	2.90060
5.000000E- 1	2.12658	6.25028	1.80916	4.70848	1.49426	3.14359
3.086583E- 1	4.48259	5.95383	3.74860	4.32814	3.06501	2.83823
1.464466E- 1	6.87865	3.59773	6.33848	2.62180	5.86710	1.78867
3.806023E- 2	1.27894E+ 1	-3.96323	1.28430E+ 1	-1.98760	1.33764E+ 1	-5.22652E- 1
LIFT	3.36784	4.21614	3.30475	3.20092	3.29693	2.18656
MOMENT	-4.10340E- 1	-2.60663	-4.81578E- 1	-1.89296	-5.36266E- 1	-1.21843

TIME= 15

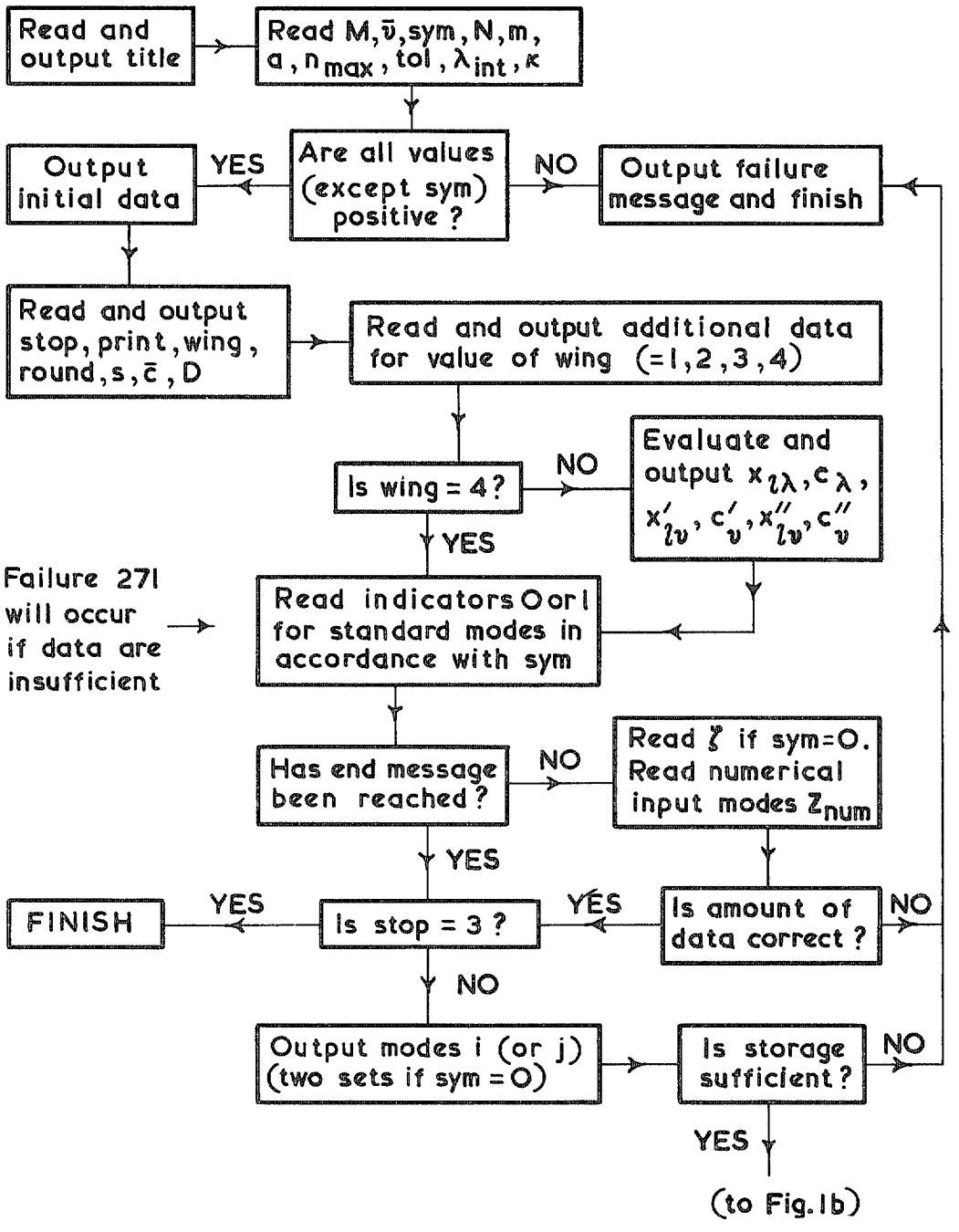

FIG. 1a. General flow diagram for Program I.

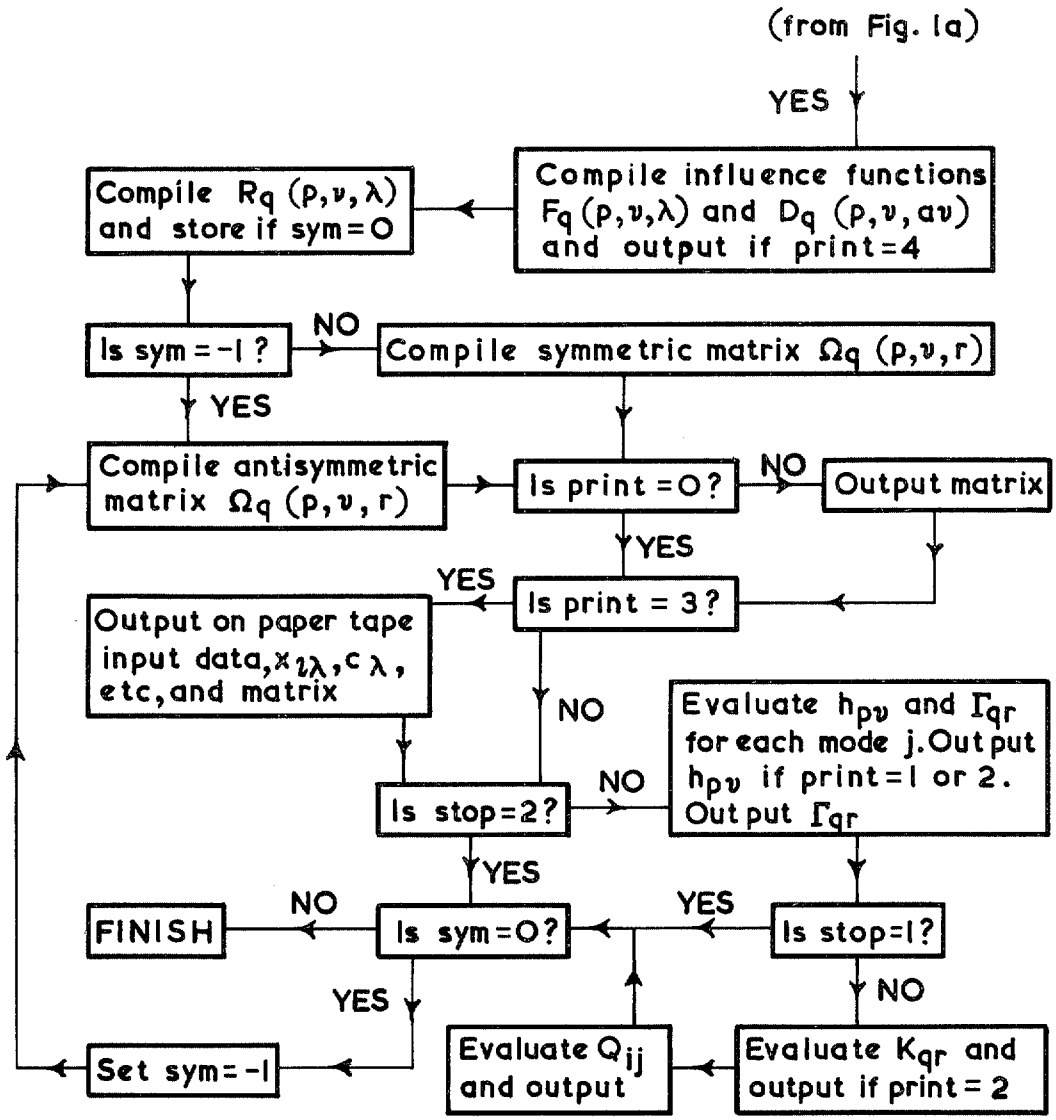

FIG. 1b. General flow diagram for Program I.

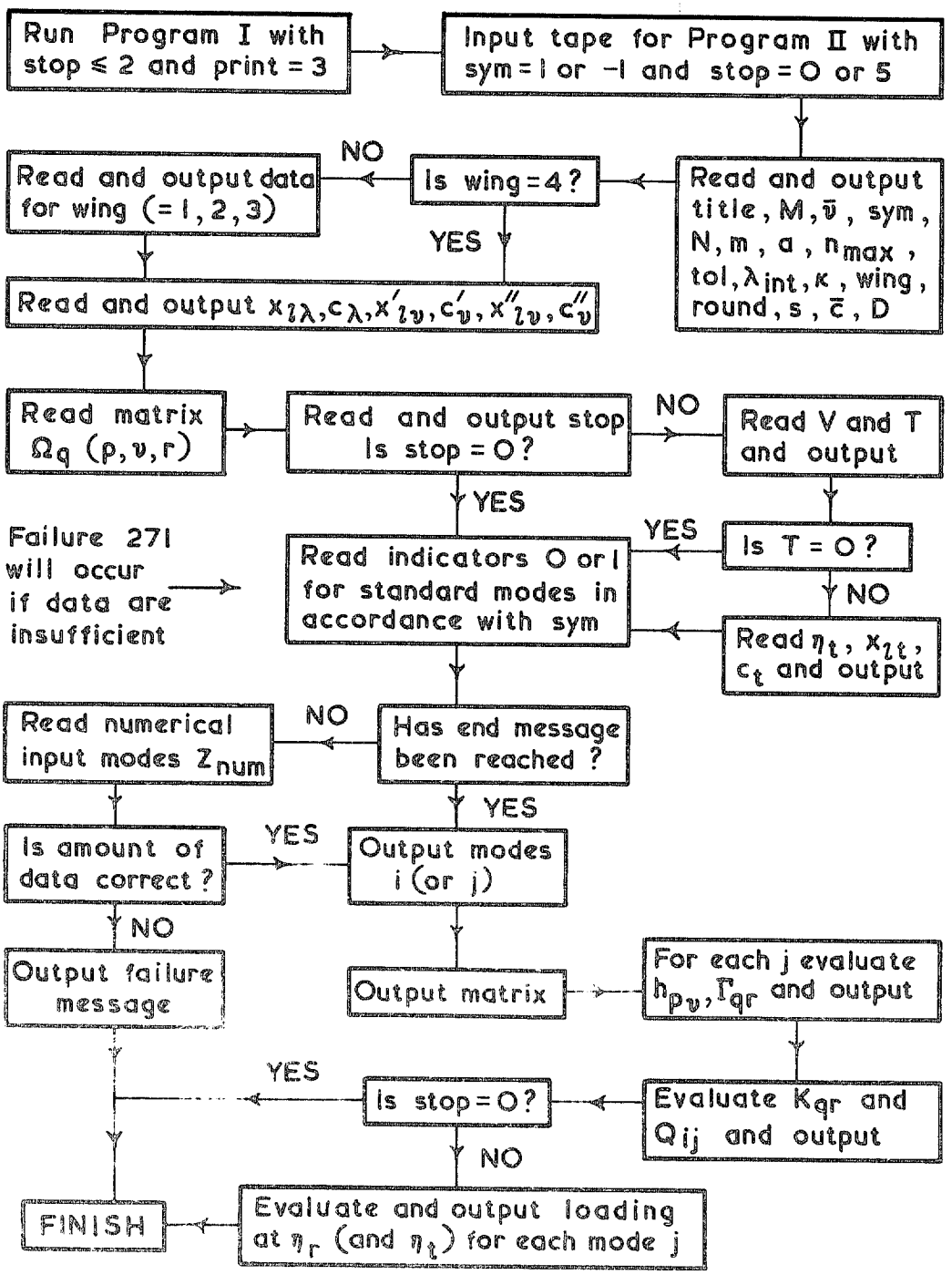

FIG. 2. General flow diagram for Program II.

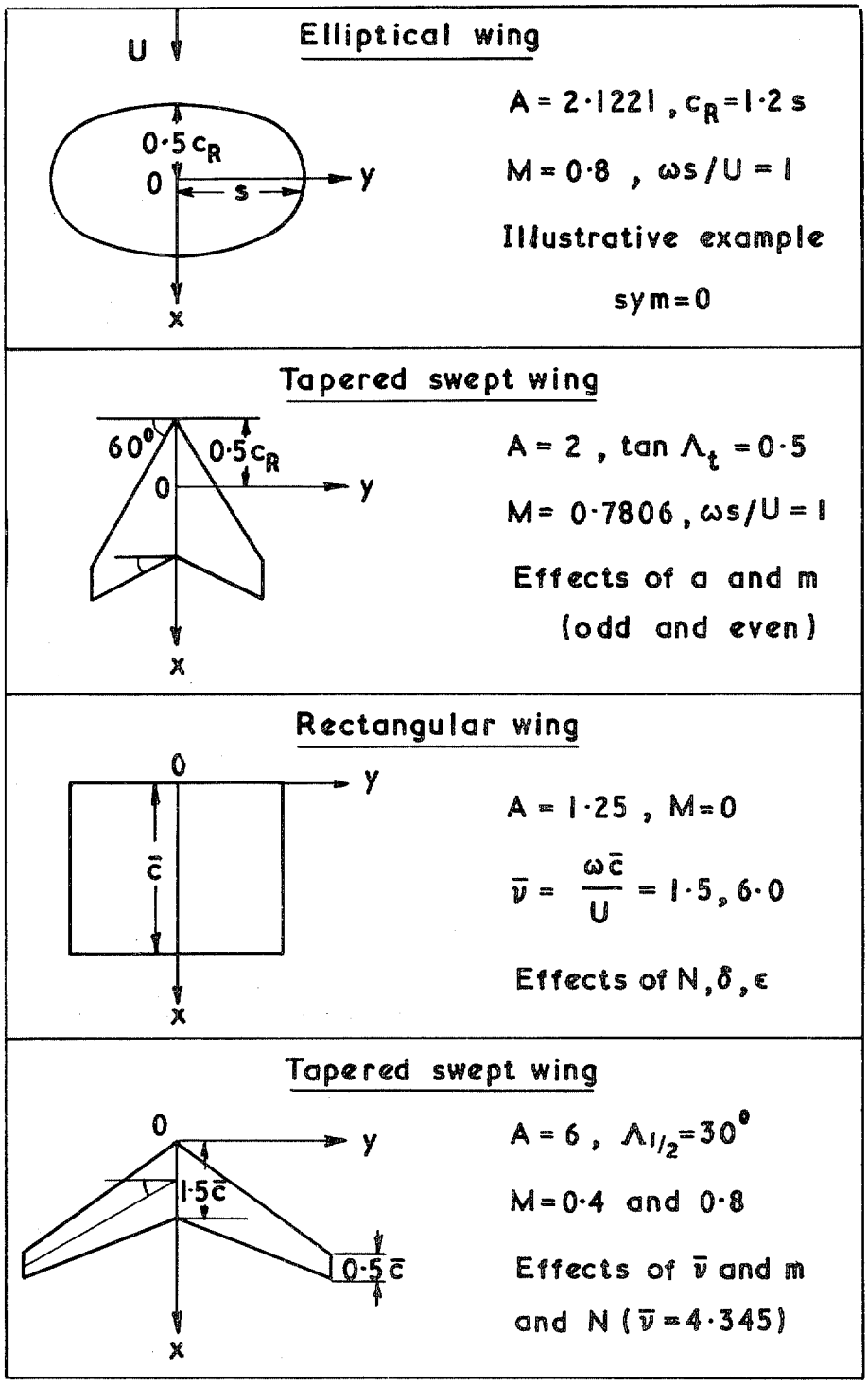

FIG. 3. Planforms and scope of calculations.

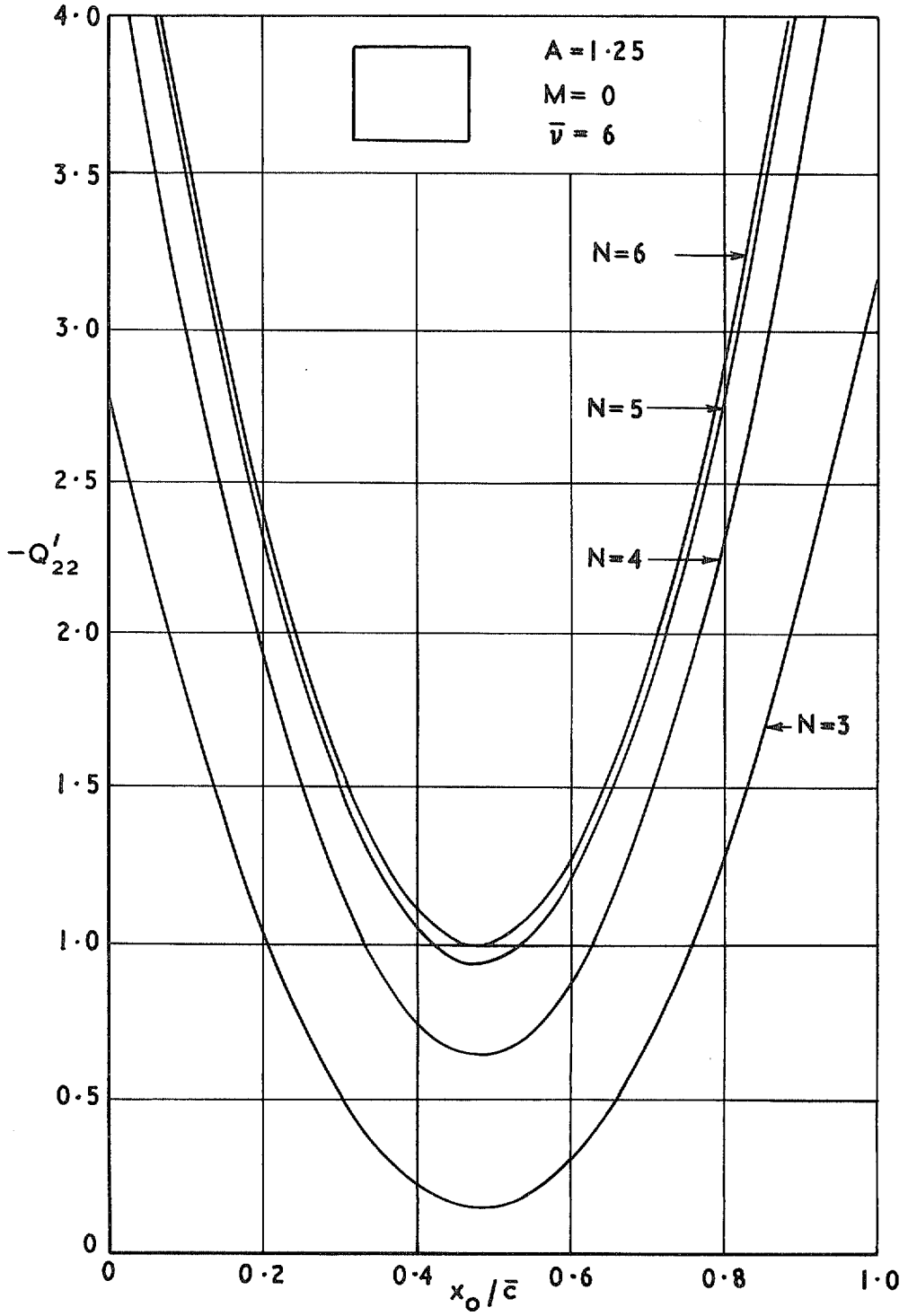

FIG. 4. Convergence with respect to N of high-frequency pitching stiffness derivative against axis position for rectangular wing.

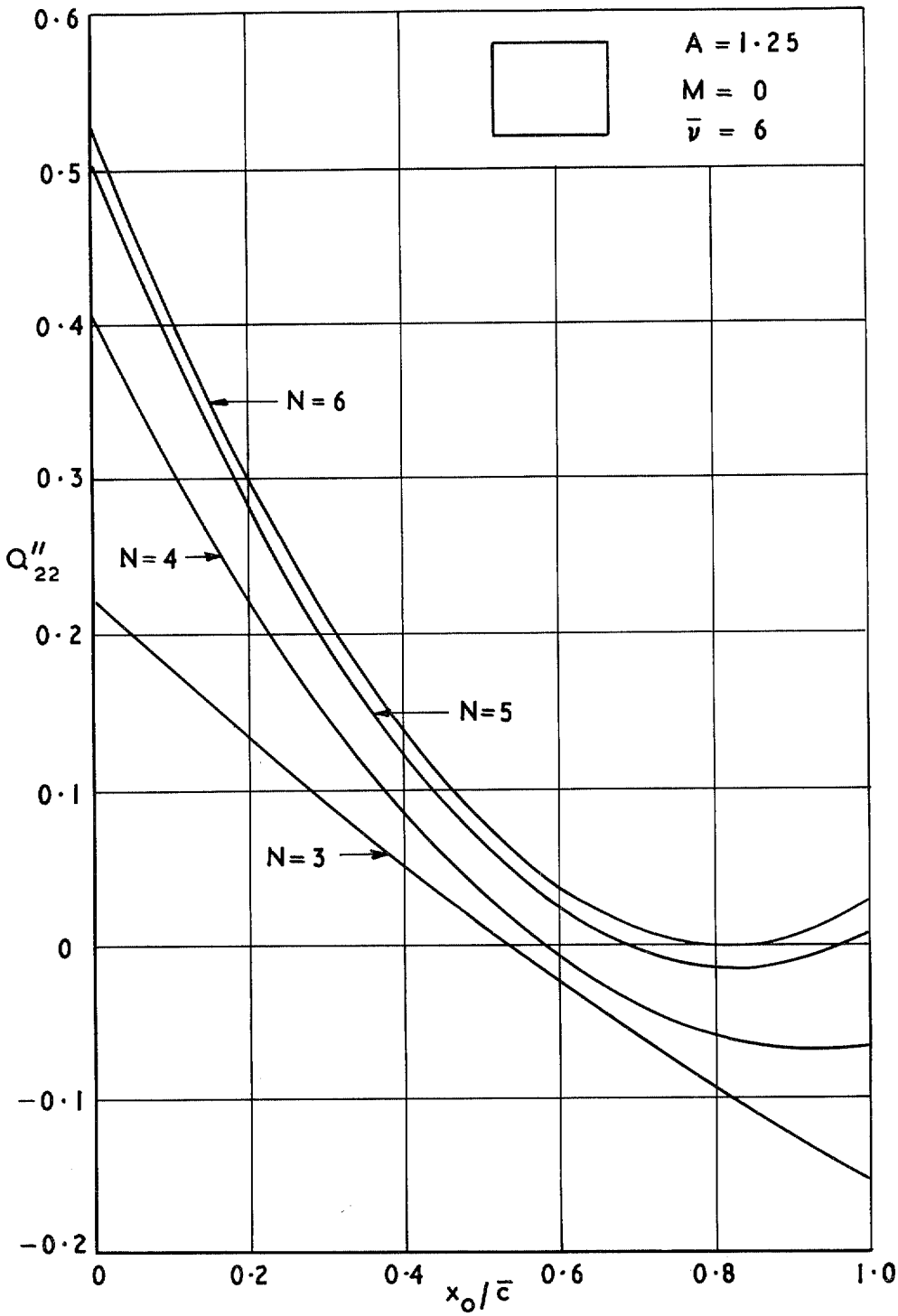

FIG. 5. Convergence with respect to N of high-frequency pitching damping derivative against axis position for rectangular wing.

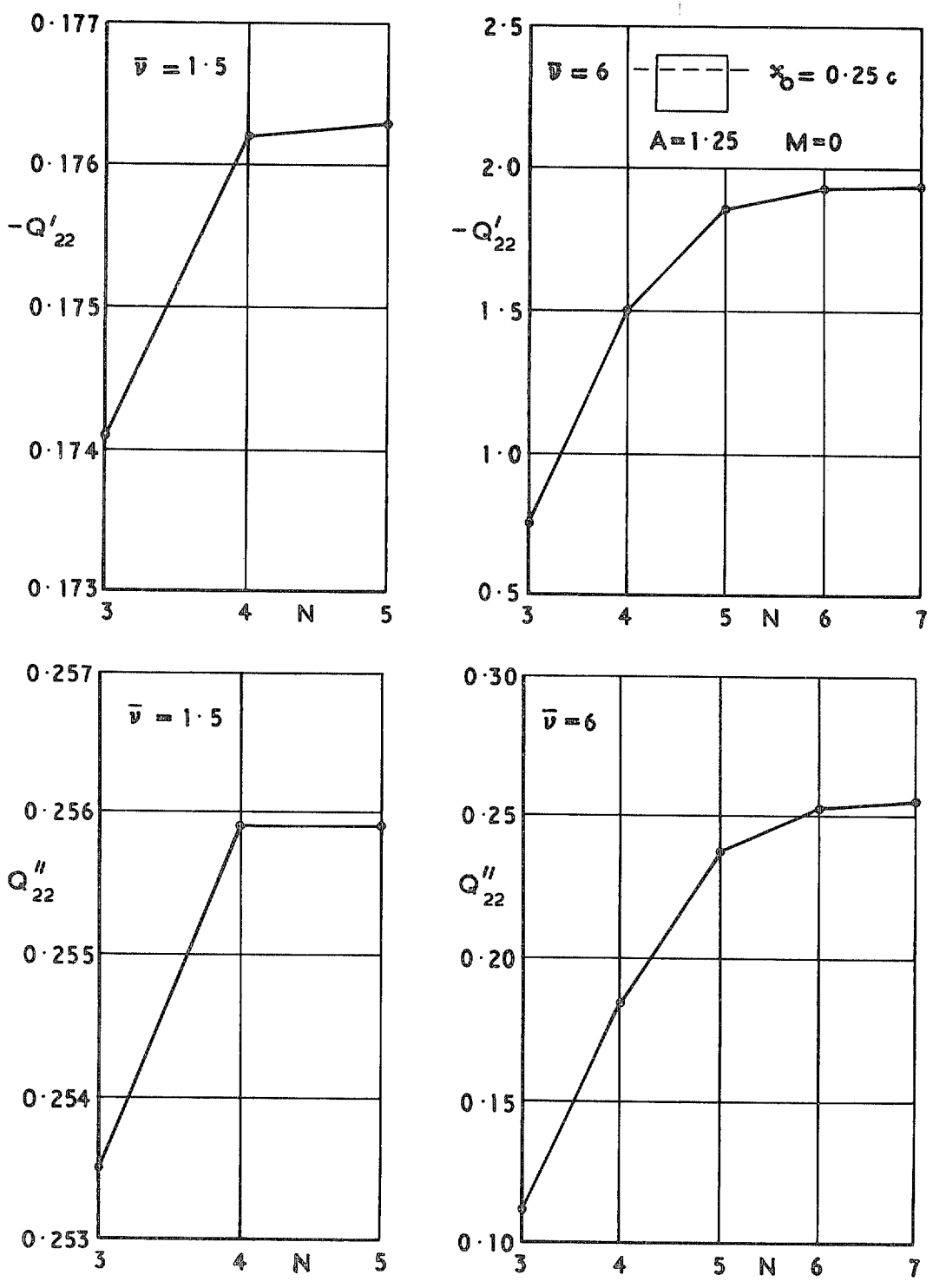

FIG. 6. Convergence with respect to N of direct pitching derivatives for rectangular wing at moderate and high frequencies.

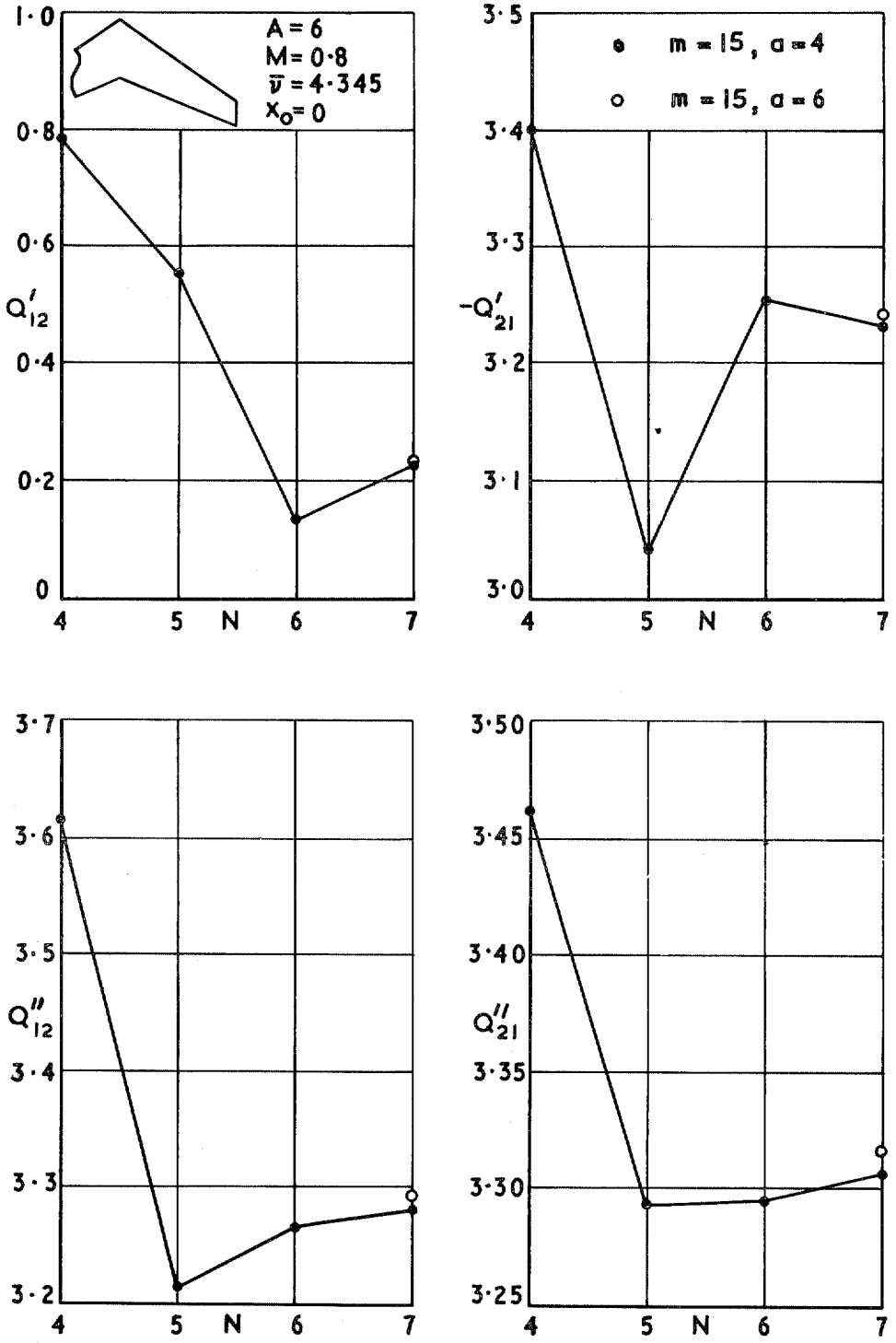

FIG. 7. Convergence with respect to N of cross derivatives for tapered swept wing at high subsonic Mach number and frequency.

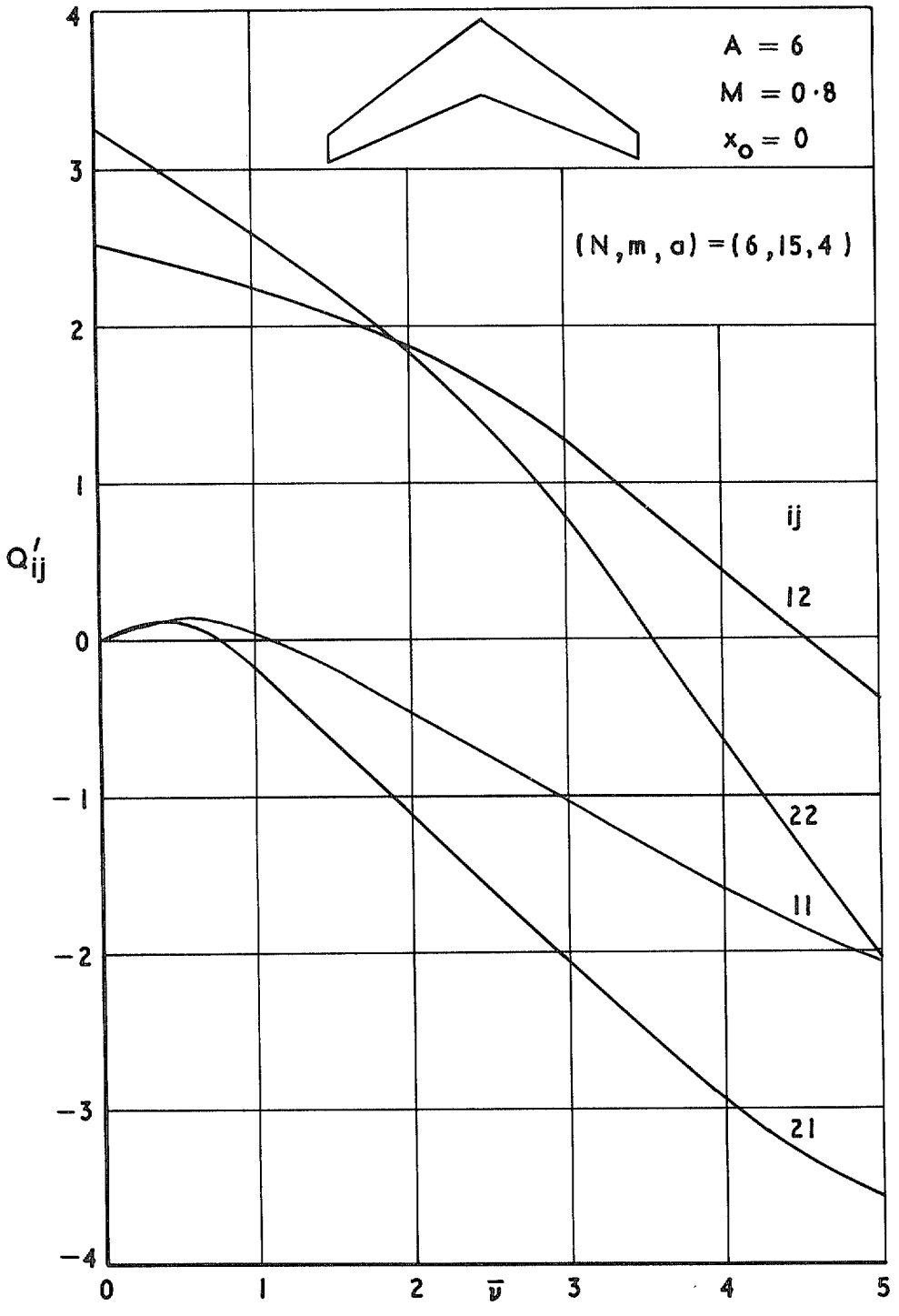

FIG. 8. Stiffness derivatives against frequency parameter for tapered swept wing at $M = 0{\cdot}8$.

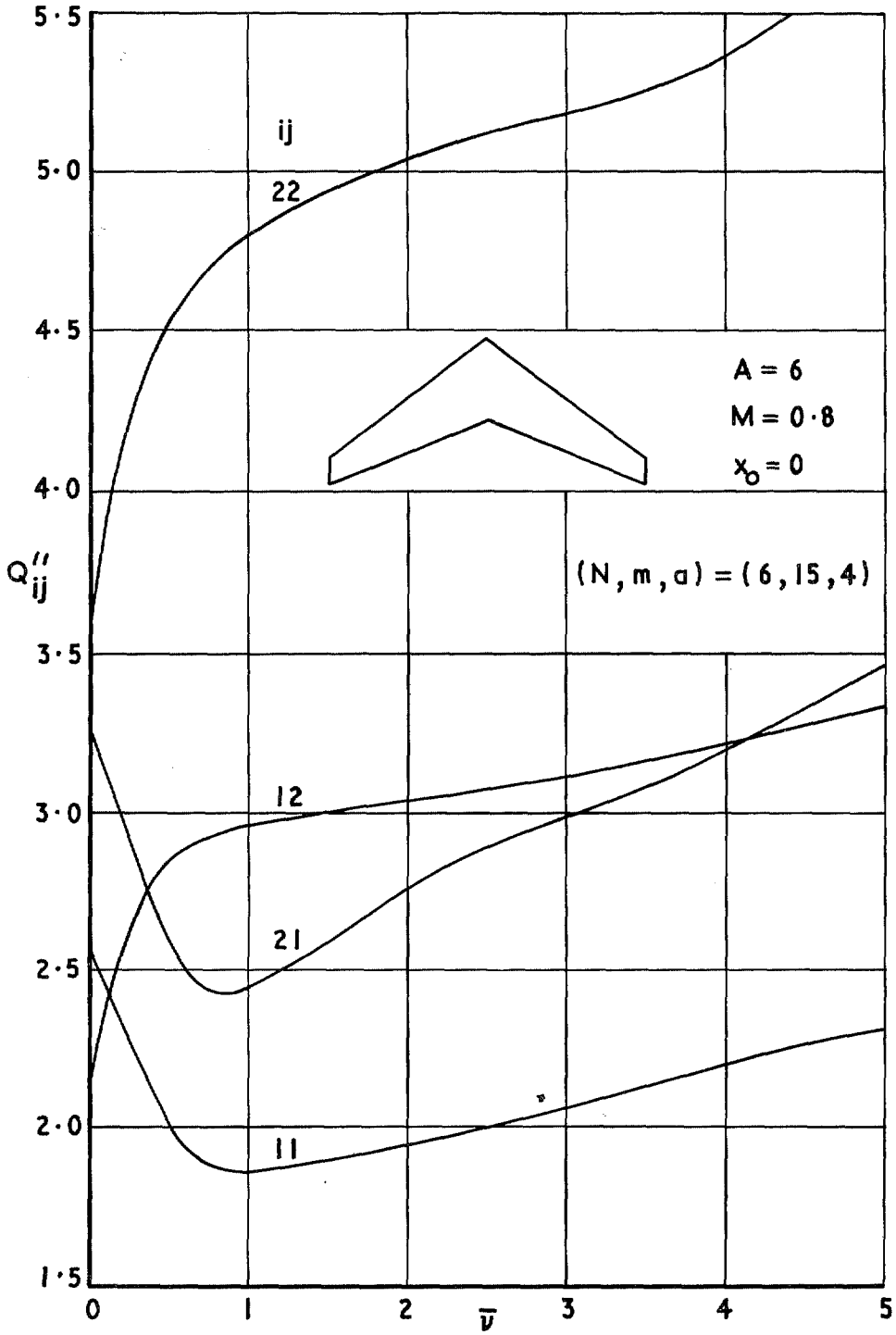

FIG. 9. Damping derivatives against frequency parameter for tapered swept wing at $M = 0{\cdot}8$.

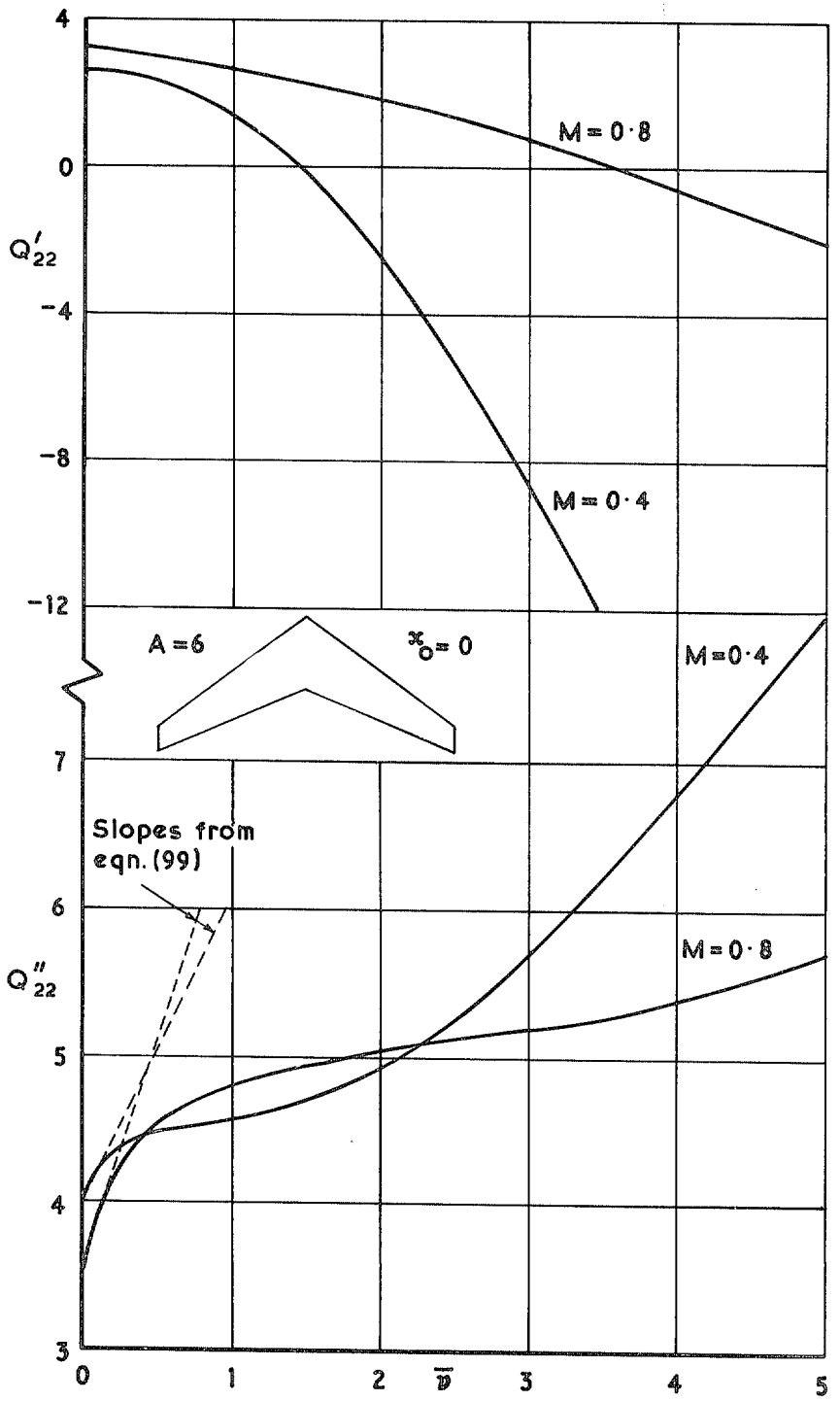

FIG. 10. Direct pitching derivatives against frequency parameter for tapered swept wing at two Mach numbers.

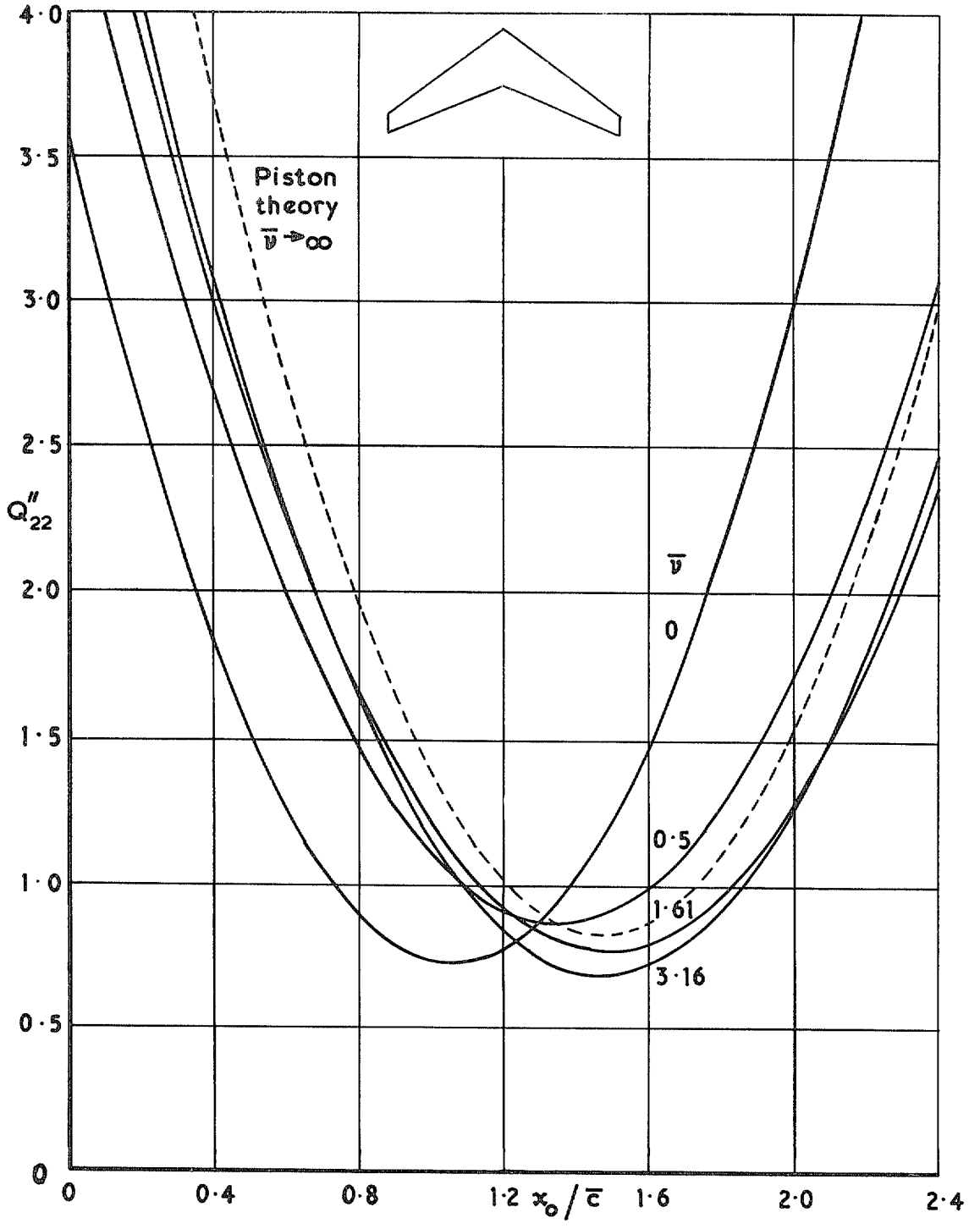

FIG. 11. Pitching damping against axis position for tapered swept wing at $M = 0{\cdot}8$ and varying frequency parameter.

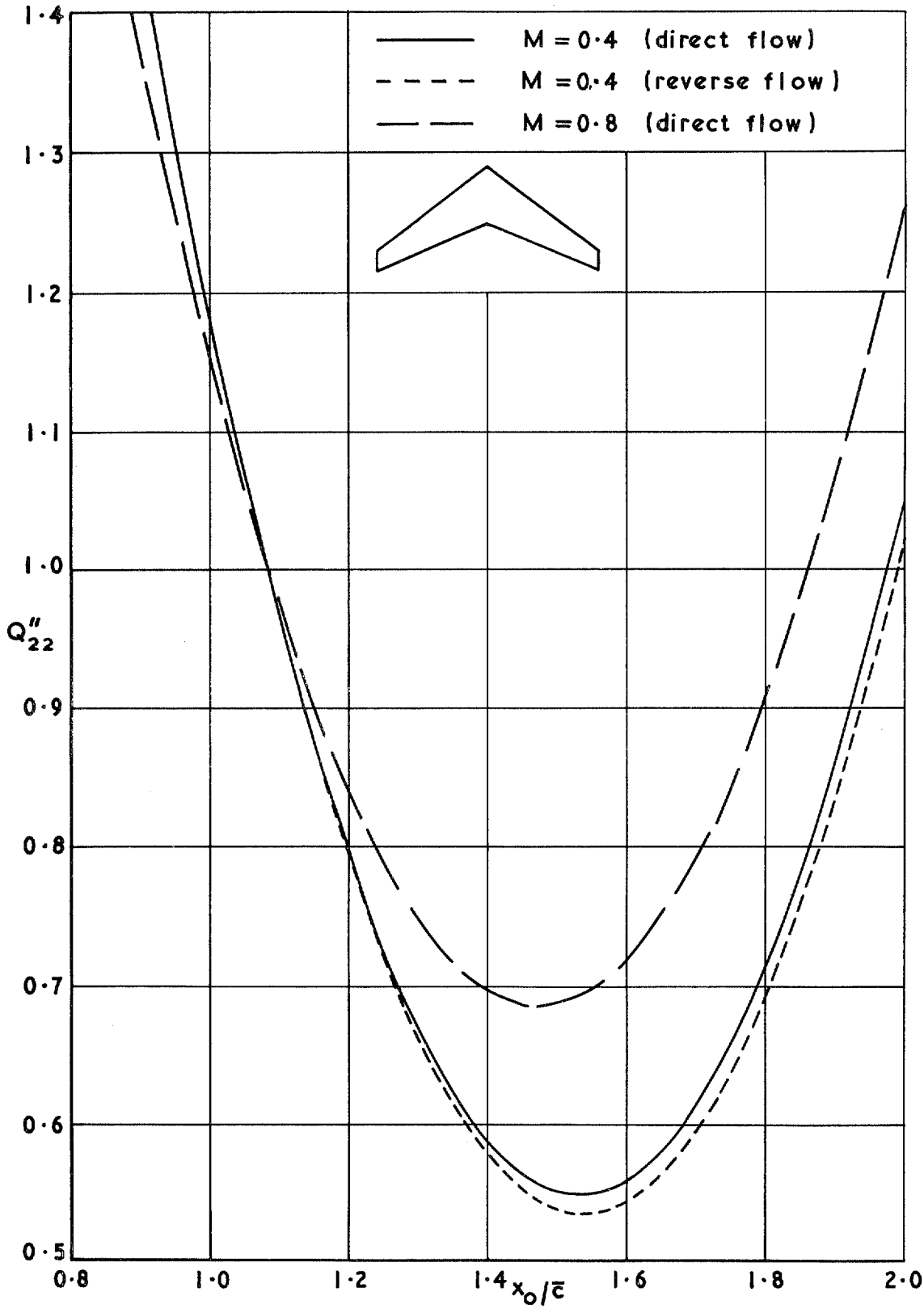

FIG. 12. Pitching damping against axis position for tapered swept wing at frequency parameter $\bar{\nu} = 3.157$.

Printed in England for Her Majesty's Stationery Office by J. W. Arrowsmith Ltd., Bristol
Dd. 503426 K.5. 11/72

HER MAJESTY'S STATIONERY OFFICE

Government Bookshops

49 High Holborn, London WC1V 6HB
13a Castle Street, Edinburgh EH2 3AR
109 St Mary Street, Cardiff CF1 1JW
Brazennose Street, Manchester M60 8AS
50 Fairfax Street, Bristol BS1 3DE
258 Broad Street, Birmingham B1 2HE
80 Chichester Street, Belfast BT1 4JY

Government publications are also available through booksellers

SBN 11 470510 0*